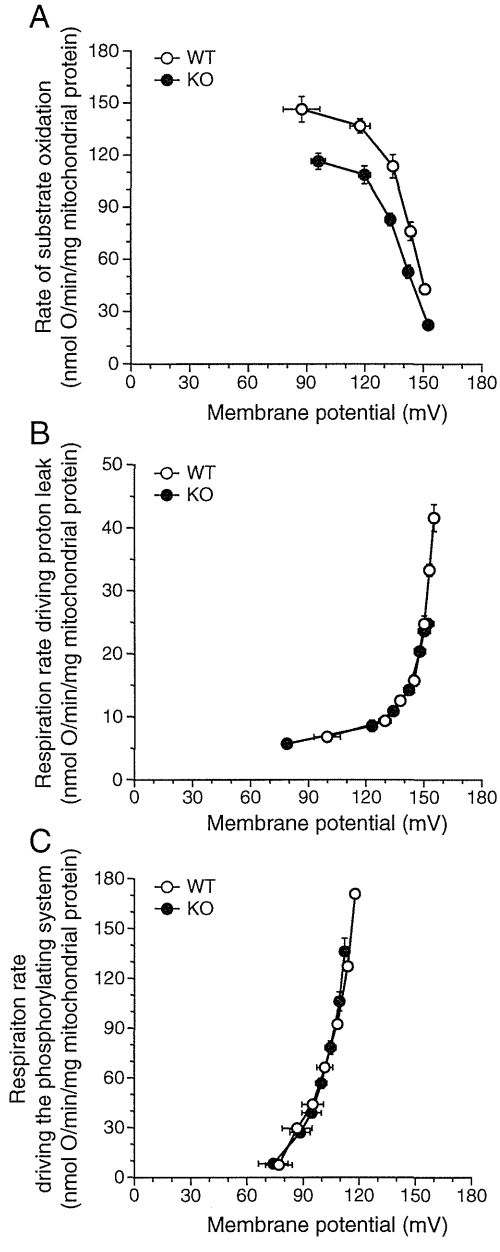

Fig. 3. Modular kinetic analysis of oxidative phosphorylation in mitochondria isolated from PINK1$^{+/+}$ and $^{-/-}$ MEFs. Modular kinetic analysis of the kinetic responses to membrane potential, $\Delta\psi$, of respiration driving (A) substrate oxidation ($\Delta\psi$ titrated with uncoupler, FCCP, starting in State 4), (B) proton leak ($\Delta\psi$ titrated with malonate, starting in State 4) and (C) the phosphorylating system, calculated by subtracting respiration driving proton leak from respiration driving the $\Delta\psi$-consumers ($\Delta\psi$ titrated with malonate starting in State 3; not shown) at each $\Delta\psi$. Open symbols, PINK1$^{+/+}$ MEFs; closed symbols, PINK1$^{-/-}$ MEFs. Error bars indicate SEM ($n=4$ independent mitochondrial preparations).

Mitochondrial ROS production

Mitochondrial ROS production rate was assessed by measurement of the H_2O_2 generation rate. Mechanisms of mitochondrial ROS production were well described elsewhere (Fig. 1 of Lambert et al., 2010). Pyruvate and malate generate NADH, which induced forward electron transport and generate ROS mainly from complex I and III. For pyruvate/malate respiration, the basal H_2O_2 generation rate (measured in the absence of respiratory chain inhibitors) was not different between PINK1$^{+/+}$ and $^{-/-}$ mitochondria (Fig. 4C). The addition of antimycin A and further addition of rotenone, which inhibited forward electron transport at complex III and I, respectively, enhanced H_2O_2 generation. During succinate respiration in the absence of respiratory chain inhibitors, ROS are generated mainly from the quinine binding site of complex I due to reverse electron flow from coenzyme Q to complex I. For succinate respiration, H_2O_2 generation rate in the absence of reparatory chain inhibitors was higher in PINK1$^{+/+}$ mitochondria than in PINK1$^{-/-}$ mitochondria, but the difference was not significant (Fig. 4D). The addition of rotenone, which blocks reverse electron flow from coenzyme Q to complex I, attenuated H_2O_2 generation.

Figs. 4 C and D show a tendency for PINK1$^{+/+}$ mitochondria to generate more ROS than PINK1$^{-/-}$ mitochondria. However, their respiration rates were remarkably different (Figs. 4A and B). Therefore, we calculated the percentage free radical leak, which is the fraction of molecules of O_2 consumed that give rise to H_2O_2 release by mitochondria (free radical leak) during either pyruvate/malate or succinate State 4 respiration (Figs. 4E and F). For pyruvate/malate respiration, mitochondria isolated from PINK1$^{-/-}$ cells had higher proportion of H_2O_2 generation than PINK1$^{+/+}$ mitochondria. During succinate respiration without respiratory inhibitors, PINK1$^{-/-}$ mitochondria had also higher proportion of free radical leak mainly from complex I due to reverse electron flow from coenzyme Q to complex I. Because the differences disappeared with addition of rotenone, which inhibit reverse electron flow, ROS generation enhanced by loss of PINK1 was mostly from complex I.

Discussion

We produced an *in vitro* model of Parkinson's disease, immortalized PINK1$^{-/-}$ MEFs. Previously, impairment of mitochondrial respiration was observed in the brains of PINK1$^{-/-}$ mice (Gautier et al., 2008). PINK1$^{-/-}$ MEFs clearly showed a phenotype of mitochondrial dysfunctions, which is consistent with PD pathogenesis. This phenotype was apparent in a cell growth experiment using medium containing galactose instead of glucose (Fig. 1B). Mitochondrial fragmentation was observed when PINK1$^{-/-}$ MEFs grew in the galactose medium (Fig. 1C), which was consistent with previous reports (Exner et al., 2007; Grünewald et al., 2009). Our results have unveiled that the PINK1$^{-/-}$ MEF line could be a potential PD model, presenting growth retardation due to decreased mitochondrial respiration activity. Thus, the PINK1$^{-/-}$ MEFs are a useful tool for evaluating the role of PINK1 in mitochondrial dysfunction and relevant to PD.

In PINK1$^{-/-}$ MEFs, mitochondrial membrane potential was decreased compared with that in littermate wild-type MEFs (Figs. 2C and D), as reported previously for PINK1 knock-down HeLa cells (Exner et al., 2007) and stable PINK1 knock-down neuroblastoma cell lines (Sandebring et al., 2009). This is a key event during elimination of mitochondria. Mitochondrial fission followed by selective fusion segregates damaged mitochondria, which decreases their membrane potential, and permits their removal by autophagy (Twig et al., 2008). The PINK1–parkin pathway is thought to have a crucial role in this mitochondrial elimination mechanism (Geisler et al., 2010; Kawajiri et al., 2010; Matsuda et al., 2010; Narendra et al., 2008, 2010; Vives-Bauza et al., 2010). To clarify what caused the decrease in mitochondrial membrane potential, we performed a modular kinetic analysis using isolated mitochondria (Fig. 3). This analyzes the kinetics of the whole of oxidative phosphorylation divided into three modules connected by their common substrate or product, mitochondrial membrane potential ($\Delta\psi$). The modules are include one $\Delta\psi$-producer (substrate oxidation) and two $\Delta\psi$-consumers (phosphorylating system and proton leak) (Brand, 1990). To decrease $\Delta\psi$, the $\Delta\psi$-producer should be down-regulated and/or $\Delta\psi$-consumers should be up-regulated. As cellular ATP levels were decreased compared with those in littermate wild-type MEFs (Fig. 2B), it is unlikely that the phosphorylating system is up-regulated. Indeed, the kinetics of the phosphorylation module were not altered (Fig. 3C). The other $\Delta\psi$-consumer, proton leak,

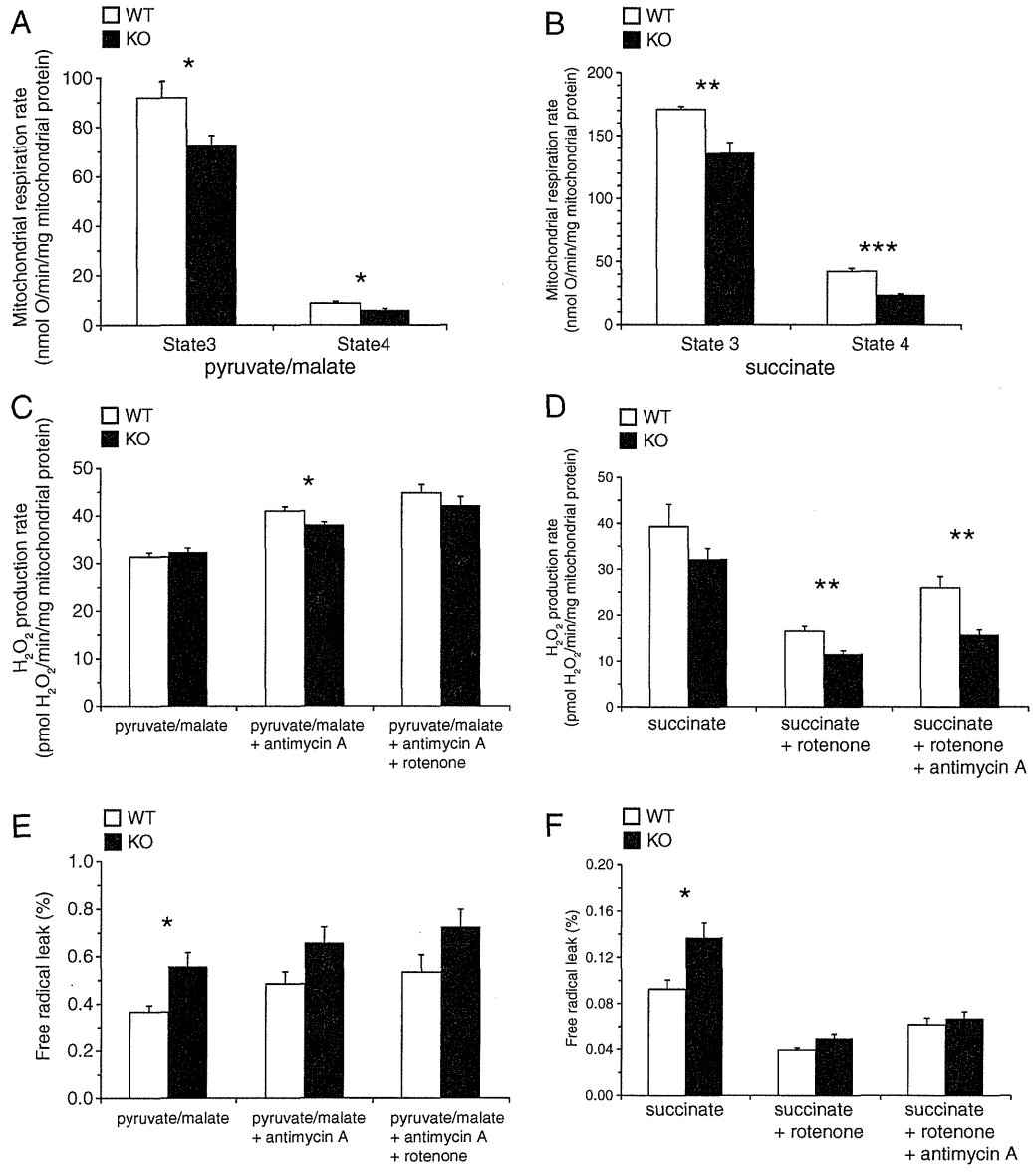

Fig. 4. Oxygen consumption rate and H_2O_2 production rate of mitochondria isolated from PINK1$^{+/+}$ and $^{-/-}$ MEFs. Open bars, PINK1$^{+/+}$ MEFs; closed bars, PINK1$^{-/-}$ MEFs. (A) State 3 and State 4 respiration rate of mitochondria with pyruvate/malate as a respiratory substrate. (B) State 3 and State 4 respiration rate of mitochondria with succinate as a respiratory substrate. Data were derived from the results of modular kinetic analysis (Fig. 3). State 3 respiration rates were the kinetic start points of the $\Delta\psi$-consumers (the sum of the phosphorylating system and proton leak). State 4 respiration rates were average values of the respiration rates at the kinetic start points of substrate oxidation and proton leak. (C, D) Mitochondrial H_2O_2 production rate with pyruvate/malate (C) or succinate (D) as a respiratory substrate. (E, F) Percentage free radical leak (FRL) for State 4 respiration with pyruvate/malate (E) or succinate (F) as a respiratory substrate. Error bars indicate SEM ($n=5$ and 4 independent mitochondrial preparations for pyruvate/malate and succinate respiration, respectively). *$P<0.05$; **$P<0.01$; ***$P<0.001$.

which partially dissipates the membrane potential without ATP synthesis, was also not changed (Fig. 3B). Therefore, the decrease in membrane potential caused by loss of PINK1 is likely to have been caused only by lower activity of the $\Delta\psi$-producer, substrate oxidation (Fig. 3A). This is the first report showing that mitochondrial membrane potential decrease caused by loss of PINK1, which is the key event for the following mitochondrial elimination, was not due to proton leak, but to respiratory chain defects. We used only succinate (a complex II-linked substrate) as a respiratory substrate in the modular kinetic analysis for technical reasons. However, complex I-linked respiration (pyruvate/malate) was also decreased in PINK1$^{-/-}$ MEFs like succinate respiration (Fig. 4A).

The mitochondrial respiration rates in State 4 were decreased in PINK1$^{-/-}$ MEFs, and consequently, the proportions of free radical leak were significantly higher in PINK1$^{-/-}$ MEFs than in PINK1$^{+/+}$ MEFs (Figs. 4E and F). Because the differences disappeared with addition of rotenone (complex I inhibitor, which inhibits reverse electron flow from coenzyme Q to complex I), ROS generation enhanced by loss of PINK1 was mostly from complex I. These results are partially consistent with those in previous reports, suggesting that MPTP and rotenone induce neuronal cell death by inhibiting complex I activity, leading to a PD-like phenotype (Dauer and Przedborski, 2003; Jackson-Lewis and Przedborski, 2007; Trojanowski, 2003).

In this study, we developed an *in vitro* PD model, the PINK1$^{-/-}$ MEF line, and established the experimental conditions for cell growth to detect mitochondrial dysfunction. This is the first report showing that complete ablation of PINK1 causes a decrease in mitochondrial membrane potential, which is not due to proton leak, but to respiratory chain defects.

Supplementary materials related to this article can be found online at doi:10.1016/j.nbd.2010.08.027.

Acknowledgments

This work was supported by a Grant-in-Aid for Scientific Research for Young Scientists (B) from JSPS (T.A. and S.Saiki), a JSPS fellowship (T.A.), Nagao Memorial Fund (S. Saiki) and a Grant from Takeda Scientific Foundation (S. Saiki and T.A.). We thank Dr. Noriyuki Matsuda for assistance to obtain immortalized cells.

References

Abou-Sleiman, P.M., Muqit, M.M., Wood, N.W., 2006. Expanding insights of mitochondrial dysfunction in Parkinson's disease. Nat. Rev. Neurosci. 7, 207–219.

Amo, T., Brand, M.D., 2007. Were inefficient mitochondrial haplogroups selected during migrations of modern humans? A test using modular kinetic analysis of coupling in mitochondria from cybrid cell lines. Biochem. J. 404, 345–351.

Barja, G., Cadenas, S., Rojas, C., Pérez-Campo, R., López-Torres, M., 1994. Low mitochondrial free radical production per unit O_2 consumption can explain the simultaneous presence of high longevity and high aerobic metabolic rate in birds. Free Radic. Res. 21, 317–327.

Brand, M.D., 1990. The proton leak across the mitochondrial inner membrane. Biochim. Biophys. Acta 1018, 128–133.

Brand, M.D., 1995. Measurement of mitochondrial protonmotive force. In: Brown, G.C., Cooper, C.E. (Eds.), Bioenergetics, a practical approach. IRL Press, Oxford, pp. 39–62.

Brand, M.D., 1998. Top-down elasticity analysis and its application to energy metabolism in isolated mitochondria and intact cells. Mol. Cell. Biochem. 184, 13–20.

Brand, M.D., Chien, L.F., Diolez, P., 1994. Experimental discrimination between proton leak and redox slip during mitochondrial electron transport. Biochem. J. 297, 27–29.

Chu, C.T., 2010. Tickled PINK1: mitochondrial homeostasis and autophagy in recessive Parkinsonism. Biochim. Biophys. Acta 1802, 20–28.

Clark, I.E., Dodson, M.W., Jiang, C., Cao, J.H., Huh, J.R., Seol, J.H., Yoo, S.J., Hay, B.A., Guo, M., 2006. *Drosophila pink1* is required for mitochondrial function and interacts genetically with *parkin*. Nature 441, 1162–1166.

Dauer, W., Przedborski, S., 2003. Parkinson's disease: mechanisms and models. Neuron 39, 889–909.

Exner, N., Treske, B., Paquet, D., Holmstrom, K., Schiesling, C., Gispert, S., Carballo-Carbajal, I., Berg, D., Hoepken, H.H., Gasser, T., Krüger, R., Winklhofer, K.F., Vogel, F., Reichert, A.S., Auburger, G., Kahle, P.J., Schmid, B., Haass, C., 2007. Loss-of-function of human PINK1 results in mitochondrial pathology and can be rescued by parkin. J. Neurosci. 27, 12413–12418.

Gandhi, S., Wood-Kaczmar, A., Yao, Z., Plun-Favreau, H., Deas, E., Klupsch, K., Downward, J., Latchman, D.S., Tabrizi, S.J., Wood, N.W., Duchen, M.R., Abramov, A.Y., 2009. PINK1-associated Parkinson's disease is caused by neuronal vulnerability to calcium-induced cell death. Mol. Cell 33, 627–638.

Gautier, C.A., Kitada, T., Shen, J., 2008. Loss of PINK1 causes mitochondrial functional defects and increased sensitivity to oxidative stress. Proc. Natl. Acad. Sci. U. S. A. 105, 11364–11369.

Geisler, S., Holmström, K.M., Skujat, D., Fiesel, F.C., Rothfuss, O.C., Kahle, P.J., Springer, W., 2010. PINK1/Parkin-mediated mitophagy is dependent on VDAC1 and p62/SQSTM1. Nat. Cell Biol. 12, 119–131.

Gispert, S., Ricciardi, F., Kurz, A., Azizov, M., Hoepken, H.H., Becker, D., Voos, W., Leuner, K., Müller, W.E., Kudin, A.P., Kunz, W.S., Zimmermann, A., Roeper, J., Wenzel, D., Jendrach, M., García-Arencíbia, M., Fernández-Ruiz, J., Huber, L., Rohrer, H., Barrera, M., Reichert, A.S., Rüb, U., Chen, A., Nussbaum, R.L., Auburger, G., 2009. Parkinson phenotype in aged PINK1-deficient mice is accompanied by progressive mitochondrial dysfunction in absence of neurodegeneration. PLoS One 4, e5777.

Grünewald, A., Gegg, M.E., Taanman, J.W., King, R.H., Kock, N., Klein, C., Schapira, A.H., 2009. Differential effects of PINK1 nonsense and missense mutations on mitochondrial function and morphology. Exp. Neurol. 219, 266–273.

Haque, M.E., Thomas, K.J., D'Souza, C., Callaghan, S., Kitada, T., Slack, R.S., Fraser, P., Cookson, M.R., Tandon, A., Park, D.S., 2008. Cytoplasmic Pink1 activity protects neurons from dopaminergic neurotoxin MPTP. Proc. Natl. Acad. Sci. U. S. A. 105, 1716–1721.

Hofhaus, G., Johns, D.R., Hurko, O., Attardi, G., Chomyn, A., 1996. Respiration and growth defects in transmitochondrial cell lines carrying the 11778 mutation associated with Leber's hereditary optic neuropathy. J. Biol. Chem. 271, 13155–13161.

Jackson-Lewis, V., Przedborski, S., 2007. Protocol for the MPTP mouse model of Parkinson's disease. Nat. Protoc. 2, 141–151.

Kawajiri, S., Saiki, S., Sato, S., Sato, F., Hatano, T., Eguchi, H., Hattori, N., 2010. PINK1 is recruited to mitochondria with parkin and associates with LC3 in mitophagy. FEBS Lett. 584, 1073–1079.

Kim, Y., Park, J., Kim, S., Song, S., Kwon, S.K., Lee, S.H., Kitada, T., Kim, J.M., Chung, J., 2008. PINK1 controls mitochondrial localization of Parkin through direct phosphorylation. Biochem. Biophys. Res. Commun. 377, 975–980.

King, M.P., Attardi, G., 1989. Human cells lacking mtDNA: repopulation with exogenous mitochondria by complementation. Science 246, 500–503.

Lambert, A.J., Buckingham, J.A., Boysen, H.M., Brand, M.D., 2010. Low complex I content explains the low hydrogen peroxide production rate of heart mitochondria from the long-lived pigeon, Columba livia. Aging Cell 9, 78–91.

Liu, W., Vives-Bauza, C., Acin-Perez, R., Yamamoto, A., Tan, Y., Li, Y., Magrane, J., Stavarache, M.A., Shaffer, S., Chang, S., Kaplitt, M.G., Huang, X.Y., Beal, M.F., Manfredi, G., Li, C., 2009. PINK1 defect causes mitochondrial dysfunction, proteasomal deficit and alpha-synuclein aggregation in cell culture models of Parkinson's disease. PLoS One 4, e4597.

Matsuda, N., Sato, S., Shiba, K., Okatsu, K., Saisho, K., Gautier, C.A., Sou, Y.S., Saiki, S., Kawajiri, S., Sato, F., Kimura, M., Komatsu, M., Hattori, N., Tanaka, K., 2010. PINK1 stabilized by mitochondrial depolarization recruits Parkin to damaged mitochondria and activates latent Parkin for mitophagy. J. Cell Biol. 189, 211–221.

Narendra, D., Tanaka, A., Suen, D.F., Youle, R.J., 2008. Parkin is recruited selectively to impaired mitochondria and promotes their autophagy. J. Cell Biol. 183, 795–803.

Narendra, D.P., Jin, S.M., Tanaka, A., Suen, D.F., Gautier, C.A., Shen, J., Cookson, M.R., Youle, R.J., 2010. PINK1 is selectively stabilized on impaired mitochondria to activate Parkin. PLoS Biol. 8, e1000298.

Park, J., Lee, S.B., Lee, S., Kim, Y., Song, S., Kim, S., Bae, E., Kim, J., Shong, M., Kim, J.M., Chung, J., 2006. Mitochondrial dysfunction in *Drosophila PINK1* mutants is complemented by *parkin*. Nature 441, 1157–1161.

Pridgeon, J.W., Olzmann, J.A., Chin, L.S., Li, L., 2007. PINK1 protects against oxidative stress by phosphorylating mitochondrial chaperone TRAP1. PLoS Biol. 5, e172.

Reitzer, L.J., Wice, B.M., Kennell, D., 1979. Evidence that glutamine, not sugar, is the major energy source for cultured HeLa cells. J. Biol. Chem. 254, 2669–2676.

Reynafarje, B., Costa, L.E., Lehninger, A.L., 1985. O_2 solubility in aqueous media determined by a kinetic method. Anal. Biochem. 145, 406–418.

Sandebring, A., Thomas, K.J., Beilina, A., van der Brug, M., Cleland, M.M., Ahmad, R., Miller, D.W., Zambrano, I., Cowburn, R.F., Behbahani, H., Cedazo-Mínguez, A., Cookson, M.R., 2009. Mitochondrial alterations in PINK1 deficient cells are influenced by calcineurin-dependent dephosphorylation of dynamin-related protein 1. PLoS One 4, e5701.

Trojanowski, J.Q., 2003. Rotenone neurotoxicity: a new window on environmental causes of Parkinson's disease and related brain amyloidoses. Exp. Neurol. 179, 6–8.

Twig, G., Elorza, A., Molina, A.J., Mohamed, H., Wikstrom, J.D., Walzer, G., Stiles, L., Haigh, S.E., Katz, S., Las, G., Alroy, J., Wu, M., Py, B.F., Yuan, J., Deeney, J.T., Corkey, B. E., Shirihai, O.S., 2008. Fission and selective fusion govern mitochondrial segregation and elimination by autophagy. EMBO J. 27, 433–446.

Valente, E.M., Abou-Sleiman, P.M., Caputo, V., Muqit, M.M., Harvey, K., Gispert, S., Ali, Z., Del Turco, D., Bentivoglio, A.R., Healy, D.G., Albanese, A., Nussbaum, R., González-Maldonado, R., Deller, T., Salvi, S., Cortelli, P., Gilks, W.P., Latchman, D.S., Harvey, R.J., Dallapiccola, B., Auburger, G., Wood, N.W., 2004. Hereditary early-onset Parkinson's disease caused by mutations in *PINK1*. Science 304, 1158–1160.

Vives-Bauza, C., Zhou, C., Huang, Y., Cui, M., de Vries, R.L., Kim, J., May, J., Tocilescu, M.A., Liu, W., Ko, H.S., Magrane, J., Moore, D.J., Dawson, V.L., Grailhe, R., Dawson, T.M., Li, C., Tieu, K., Przedborski, S., 2010. PINK1-dependent recruitment of Parkin to mitochondria in mitophagy. Proc. Natl. Acad. Sci. U. S. A. 107, 378–383.

Wood-Kaczmar, A., Gandhi, S., Yao, Z., Abramov, A.Y., Miljan, E.A., Keen, G., Stanyer, L., Hargreaves, I., Klupsch, K., Deas, E., Downward, J., Mansfield, L., Jat, P., Taylor, J., Heales, S., Duchen, M.R., Latchman, D., Tabrizi, S.J., Wood, N.W., 2008. PINK1 is necessary for long term survival and mitochondrial function in human dopaminergic neurons. PLoS One 3, e2455.

Yang, Y., Ouyang, Y., Yang, L., Beal, M.F., McQuibban, A., Vogel, H., Lu, B., 2008. Pink1 regulates mitochondrial dynamics through interaction with the fission/fusion machinery. Proc. Natl. Acad. Sci. U. S. A. 105, 7070–7075.

AUTHOR QUERY FORM

ELSEVIER	**Journal:** TIPS **Article Number:** 898	**Please e-mail or fax your responses and any corrections to:** **E-mail:** corrections.esnl@elsevier.thomsondigital.com **Fax:** + 31 20 485 2521

Dear Author,

Please check your proof carefully and mark all corrections at the appropriate place in the proof (e.g., by using on-screen annotation in the PDF file) or compile them in a separate list. To ensure fast publication of your paper please return your corrections within 48 hours.

For correction or revision of any artwork, please consult http://www.elsevier.com/artworkinstructions.

Please note that the figure resolution in these proofs is lower than the original figures to avoid problems with emailing large file sizes. The figure resolution in the final publication will be equivalent to the original figure submission.

Any queries or remarks that have arisen during the processing of your manuscript are listed below and highlighted by flags in the proof. Click on the 'Q' link to go to the location in the proof.

Location in article	Query / Remark: click on the Q link to go Please insert your reply or correction at the corresponding line in the proof
Q1	what does this refer to?

Thank you for your assistance.

Review

Cell PRESS

Genetic mutations and functions of PINK1

Sumihiro Kawajiri, Shinji Saiki, Shigeto Sato and Nobutaka Hattori

Department of Neurology, Juntendo University School of Medicine, 2-1-1 Hongo, Bunkyo-ku, Tokyo, 113-8421, Japan

Parkinson's disease (PD) is the second most common neurodegenerative disease. Mutations in *PINK1* (*PARK6*) are the second most frequent cause of autosomal recessive, young-onset PD, after *parkin* (*PARK2*). PINK1 (a kinase with an N-terminal mitochondrial targeting sequence) provides protection against mitochondrial dysfunction and regulates mitochondrial morphology via fission/fusion machinery. PINK1 also acts upstream of parkin (a cytosolic E3 ubiquitin ligase) in a common pathway. Recent studies have described PINK1/parkin function in the maintenance of mitochondrial quality via autophagy (mitophagy). PINK1/parkin-mediated mitophagy provides new insights into the etiology of PD and could be a suitable target for new treatment of PD. In this review, we discuss the molecular genetics and functions of PINK1, which could be key factors in novel rational therapy for sporadic PD as well as *PINK1*-linked PD.

Parkinson's disease (PD)

PD is the second most common neurodegenerative disease worldwide after Alzheimer's disease. The prevalence of PD increases with age, and is estimated to be ~1% in those aged > 65 years [1]. The major clinical features are: (i) motor symptoms (called 'parkinsonism'), which include resting tremor, rigidity, bradykinesia (slowness in executing movement) and postural instability; and (ii) non-motor symptoms (e.g. cognitive dysfunction, autonomic nervous system dysfunction, sleep disorders). Pathological features include pronounced loss of dopaminergic neurons in the substantia nigra pars compacta and eosinophilic cytoplasmic inclusion containing α-synuclein aggregates (known as Lewy bodies) in the remaining dopaminergic neurons. No treatment is available to suppress the progression of cell death, and the goal of current therapies is only to alleviate symptoms.

The pathogenesis of PD remains unclear, although mitochondrial dysfunction due to oxidative stress has been proposed to play a major part [2]. Most cases of PD are sporadic, but ~5–10% of PD cases are hereditary. Several genes (e.g. *α-synuclein, parkin, PTEN-induced putative kinase 1* (*PINK1*), *DJ-1*, *leucine rich repeat kinase 2* (*LRRK2*)) have been identified as causative genes for familial Parkinson's disease (FPD) [3]. *PINK1*-linked PD (*PARK6*-linked PD) is the second most common autosomal recessive young-onset PD, after *parkin*-linked PD (*PARK2*-linked PD). Initial studies suggested that PINK1 provided protection against mitochondrial dysfunction [4–6]. However, the exact function of PINK1 remains unclear. Recent evidence also suggests that PINK1 plays a part in mitochondrial quality control via autophagy machinery, in collaboration with parkin (a cytosolic E3 ligase). In this review, we analyze the recent work published on PINK1 function, which can be a key factor in novel rational therapy for sporadic PD as well as *PINK1*-linked PD.

Clinical characteristics of PINK1-linked PD

Clinical features

The clinical features of *PINK1*-linked PD include parkinsonism associated with a good response to levodopa (the precursor to the dopamine), frequent occurrence of levodopa-induced dyskinesias, and infrequent occurrence of dystonia at onset, similar to those of sporadic PD. The only distinctive features are the earlier age of onset and slower progression [7]. The age of onset of *PINK1*-linked PD is around the early thirties [8,9], whereas that of sporadic PD is after the age of 60 years[1]. Unlike *parkin*-linked PD, hyperreflexia and sleep benefit are not common in *PINK1*-linked PD. However, some patients with *PINK1*-linked PD exhibit foot dystonia at onset and sleep benefit, mimicking those with *parkin*-linked PD. Others with *PINK1*-linked PD show atypical clinical features associated with psychiatric problems and dementia, both of which are rare in patients with *parkin*-linked PD.

Pathological features

As mentioned above, accumulation of Lewy bodies is the pathological hallmark of sporadic PD. Lewy bodies were also detected in the brain of a *PINK1*-linked PD patient with compound heterozygous mutations (c.1252_1488 del and c.1488 + 1G > A) [10], whereas they are absent in the brains of *parkin*-linked PD patients [11,12]. Other pathological changes seen in the PD patient with the compound heterozygous *PINK1*-mutations include neuronal loss in the substantia nigra pars compacta accompanied with astrocytic gliosis and moderate microgliosis. No apparent cell loss, Lewy bodies, or abnormal neurites are seen in the locus ceruleus. However, pathological examination has been reported in only one case of *PINK1*-linked PD, so further pathological studies are needed to determine the association between Lewy bodies and the pathogenesis of *PINK1*-linked PD.

PINK1

Molecular structure

The *PINK1* gene contains 8 exons spanning ~1.8 kilobases and encodes a 581–amino acid protein. The transcript is

Corresponding author: Hattori, N. (nhattori@juntendo.ac.jp).

0165-6147/$ – see front matter doi:10.1016/j.tips.2011.06.001 Trends in Pharmacological Sciences xx (2011) 1–8

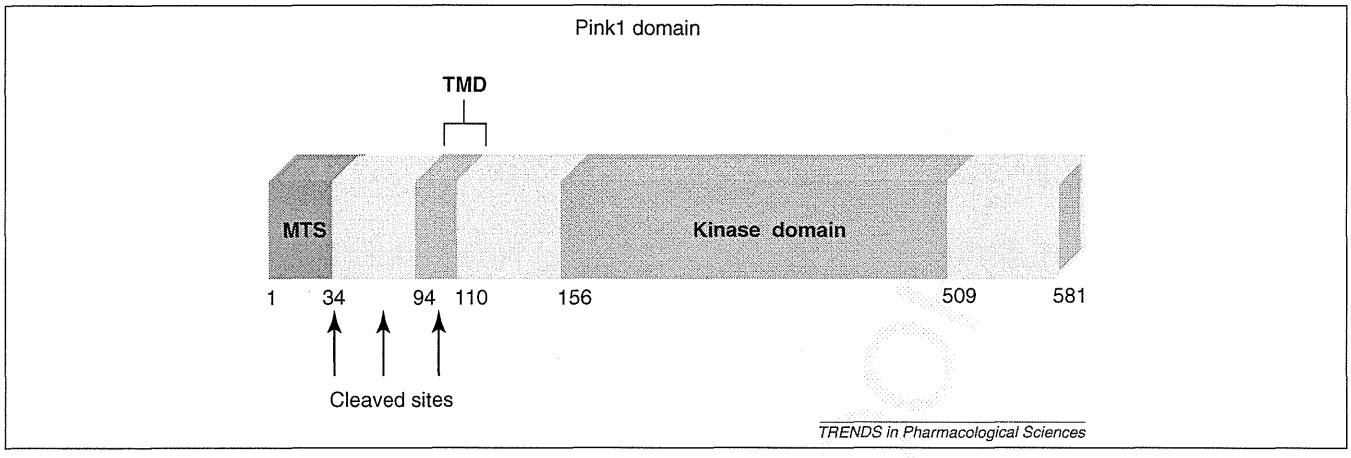

Figure 1. Putative functional domains and motifs of PINK1. Possible cleaved sites consist of the end of mitochondrial targeting sequence (MTS), sites between MTS and the transmembrane domain (TMD), and sites in the TMD.

ubiquitously expressed and predicted to encode an N-terminal 34–amino acid mitochondrial targeting sequence (MTS), a transmembrane domain (TMD) (residues 94–110) and a highly conserved protein kinase domain (residues 156–509) showing a high degree of homology to the serine/threonine kinases of the Ca^{2+}/calmodulin family [13] (Figure 1). It is important to understand the topology and subcellular distribution of PINK1 when considering PINK1 functions. PINK1 is a mitochondrial membrane integral protein whose kinase domain localizes in the outer mitochondrial membrane and is accessible from the cytoplasm. The TMD is crucial for anchoring PINK1 to the mitochondrial membrane and to ensure that the kinase domain faces the cytoplasm [14]. Subcellular fractionation shows that overexpressed PINK1 is localized in the mitochondria and cytoplasm [15], although the localization of endogenous PINK1 is not clear. This is because PINK1 is so rapidly turned over under basal conditions [16,17] that the expression level of PINK1 is very low and no antibodies against endogenous PINK1 are available. A chimeric protein consisting of a fluorescence protein fused to the N-terminus of PINK1 localizes to the mitochondria. Thus, the putative MTS of PINK1 is sufficient for its mitochondrial localization [18]. PINK1 translocated to the mitochondria by MTS is processed at several sites, such as 34 and/or 77 amino acids at the N-terminus and another site in the TMD. PINK1 mainly includes the full-length form (~63 kDa) and the cleaved form (~55 kDa) [15,18–20] (Figure 1).

Human genetics

PINK1 (PARK6) was identified in 2004 as a causative gene of autosomal recessive young-onset PD [13]. Since then, several mutations have been identified in PD patients in Europe and Japan [21]. With regard to the mode of inheritance (e.g. recessive form), loss of PINK1 function is proposed as the mechanism of *PINK1*-linked PD. The estimated prevalence of PINK1 mutations in different ethnicities is 1–8% of familial or young-onset PD [22]. Approximately 50 pathogenic mutations (missense mutations, genomic rearrangements, truncating mutations) have been identified in diverse populations. Most of the mutations are observed in the serine/threonine kinase domain, suggesting that loss of kinase activity plays a crucial part in the pathogenesis of *PINK1*-linked PD. Although the genotype–phenotype correlation has not been confirmed, the mean age at onset in patients with single heterozygous mutations is higher than that in patients with homozygous mutations [9,23]. Homozygous mutations in *PINK1* invariably cause *PINK1*-linked PD, whereas heterozygous mutations have been suggested to be a susceptibility factor for sporadic PD [24].

PINK1 function

Kinase activity

As mentioned above, PINK1 is a serine/threonine kinase protein. Several studies have reported that pathogenic mutations in PINK1, such as p.K219A, p.G309D, p.L347P, p.D362A, p.D384A, p.G386A, p.G409 V, p.E417G, are associated with reduced kinase activity [5,15,18,25]. Furthermore, the C-terminus of PINK1 regulates its kinase activity, although there is controversy over whether it up-regulates or down-regulates [18,25] activity [25]. Mutations in the PINK1 C-terminus cause early-onset parkinsonism [26]. Therefore, we have to consider the effect of the C-terminus on kinase activity to be significant. TNF receptor-associated protein 1 (TRAP1), a mitochondrial chaperone, has been identified as a PINK1 substrate. PINK1 might provide protection against oxidative stress-induced apoptosis by the phosphorylation of TRAP1 [5]. Another candidate substrate of PINK1 is parkin. The linker region of parkin is phosphorylated by PINK1, and parkin phosphorylated by PINK1 promotes its mitochondrial translocation [27]. The activity of parkin E3 ligase functions to catalyze the K63-linked polyubiquitination of IKKγ, which is a critical step in the cytoprotective signaling pathway that activates NF-κB, a ubiquitously expressed transcription of several pro-survival genes [18,28]. PINK1 is thought to modulate the phosphorylation status of another mitochondrial protein Omi/HtrA2 (a gene product for *PARK13*), possibly through indirect mechanisms [6]. Rictor, a specific component of mammalian target of rapamycin complex 2 (mTORC2), is phosphorylated by overexpression of PINK1. Enhanced Akt through activation of

mTORC2 provides cytoprotection [20,29]. These reports corroborate the fact that kinase activity has crucial roles in the pathogenesis of *PINK1*-linked PD.

Interaction with other PD-associated genes

PINK1-deficient *Drosophila* and *PINK1*-linked PD patients show very similar phenotypes, in contrast to flies and patients whose symptoms are caused by *parkin* mutations. Moreover, overexpression of parkin rescues the phenotype of *PINK1*-deficient *Drosophila*, but not *vice versa* [30,31]. However, Omi/HtrA2 is not an essential component of the PINK1/parkin pathway in *Drosophila* [32]. In cultured cells, PINK1 knockdown phenotypes are also rescued by overexpression of parkin, but not *vice versa* [33]. Parkin stabilizes PINK1 through direct interaction [34]. These results suggest that PINK1 functions upstream of parkin in a common pathway. Furthermore, parkin, PINK1, and DJ-1 form a ubiquitin E3 ligase complex that promotes the degradation of unfolded proteins [35]. In *Drosophila*, DJ-1 can rescue the consequences of PINK1 loss (except for infertility), but not the consequences of parkin loss. Furthermore, parkin cannot rescue DJ-1 loss, suggesting that DJ-1 may not be directly downstream of PINK1 [26,36]. In human neuroblastoma cells, parkin protects against the loss of DJ-1 and, although DJ-1 does not alter *PINK1*-deficient mitochondrial phenotypes, DJ-1 is active against rotenone-induced damage in the absence of PINK1 [27,37]. These findings indicate that DJ-1 works in parallel to the PINK1/parkin pathway to maintain mitochondrial function.

PINK1 knockdown causes proteasome dysfunction, accompanied by increased α-synuclein aggregation [38]. *PINK1*-deficient *Caenorhabditis elegans* exhibits a reduced length of mitochondrial cristae, increased sensitivity to paraquat (a herbicide which causes oxidative stress and parkinsonism) and defective axonal outgrowth of a pair of canal-associated neurons. In the absence of LRRK2, all these phenotypic aspects can be suppressed [39]. Furthermore, in *Drosophila*, overexpression of LRRK2 potentiates the bristle loss phenotype of PINK1 [40]. These results suggest that loss of LRRK2 suppresses the PINK1 phenotype. Taken together, evidence suggests that dysfunction of several causative gene products might contribute to the pathogenesis for PD through a common pathway (Figure 2).

Mitochondrial regulation

Mitochondrial function: In cultured cells, overexpression of PINK1 confers resistance to toxins against mitochondria such as staurosporine, 1-methyl-4-phenyl-1,2,3,6-tetrahydropyridine (MPTP), and rotenone, and PINK1 expression provides resistance to MPTP-induced dopaminergic neuronal loss in mice [4,41]. Consistent with these reports, reduction of PINK1 levels by RNA interference (RNAi) in cultured cells resulted in enhanced cell death in the presence of MPTP and rotenone [42]. In this regard, *PINK1*-deficient animal models and model-derived cells have provided important information on the endogenous function of PINK1. *PINK1*-deficient *Drosophila* showed degeneration of flight muscles, male sterility, and dopaminergic neuronal cells accompanied by mitochondrial abnormality, and shared phenotypic similarity with *parkin*-deficient *Drosophila* [30,31]. These models exhibit decreases in mitochondrial membrane potential ($\Delta\Psi m$), mitochondrial DNA, complex I, ATP, and an increased proportion of swollen mitochondria and susceptibility to apoptotic stimuli. Concomitant defects in synaptic function are also observed [43]. These results suggest that

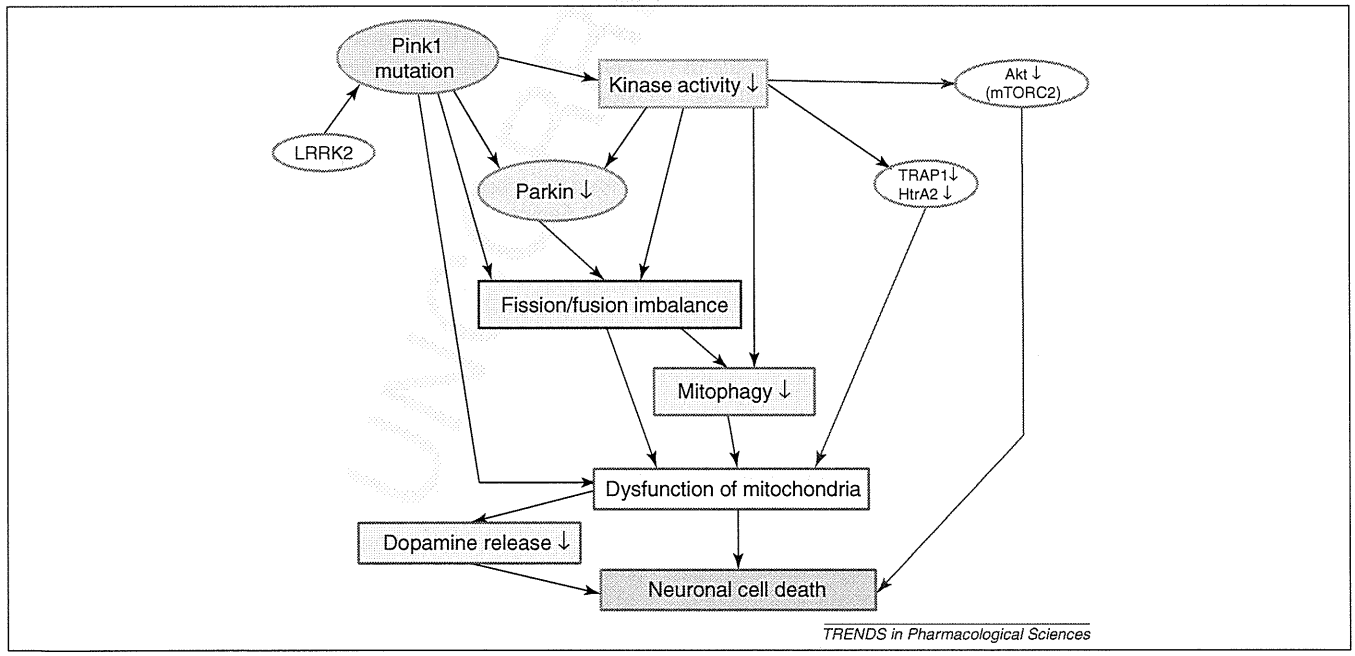

Figure 2. Proposed mechanism of *PINK1*-linked PD. Loss of PINK1 on mitochondria inhibits parkin functions and induces mitochondrial fission/fusion imbalance, which in turn causes impaired mitophagy, resulting in mitochondrial dysfunction. The kinase activity of PINK1 is important for mitophagy. Decreased dopamine release due to mitochondrial dysfunction induces neuronal cell death. Furthermore, TRAP1 and HtrA2 are not activated under reduced PINK1 kinase activity, leading to mitochondrial dysfunction. Reduced PINK1 kinase activity also results in failure of activation of Akt, leading to decreased cytoprotective function. LRRK2 exacerbates loss of PINK1.

loss of PINK1 can cause dopaminergic neuronal cell death due to functional defects in mitochondria.

In contrast, *PINK1*- and *parkin*-deficient mice do not exhibit major abnormalities, whereas absence of PINK1 causes several deficits, including: (i) reduced synaptic dopamine release and plasticity in the striatum [44]; (ii) impaired mitochondrial respiration in the striatum at 3–4 months of age and in the cerebral cortex at 2 years [45]; and (iii) progressive weight loss and selective reduction of locomotor activity for spontaneous movements in old age [46]. These findings indicate that the mitochondria in *PINK1*-deficient models are more vulnerable to aging. Primary cultured neurons derived from *PINK1*-deficient mice showed increased intracellular calcium levels and vulnerability, with subsequent excess production of reactive oxygen species (ROS), decreased glucose availability, loss of $\Delta\Psi m$ and defects of complex I, causing pathological opening of the mitochondrial permeability transition pore [47]. In *PINK1*-deficient mouse embryonic fibroblasts (MEFs), $\Delta\Psi m$ and cellular ATP levels are lower than in wild-type MEFs. However, mitochondrial proton leak (which reduces membrane potential in the absence of ATP synthesis) is not altered by loss of PINK1. Instead, low activity of the respiratory chain (which produces membrane potential oxidizing substrates using oxygen) has been observed [48]. These results suggest that decreased $\Delta\Psi m$ caused by loss of PINK1 is not due to proton leak, but to respiratory chain defects [39].

Similar to *parkin*-deficient mice, *PINK1*-deficient mice do not show prominent phenotypes. However, results from *PINK1*-deficient mice indicate that dysfunction of mitochondrial proteins (e.g. complex I) and aging are important in the pathogenesis of *PINK1*-linked PD as well as in sporadic PD.

Samples obtained from patients with hereditary PD can provide important information regarding the pathogenesis of PD. Skin fibroblasts of patients homozygous for the p.G309D *PINK1* mutation show: (i) a mild decrease in complex I activity and a trend of superoxide elevation [49]; (ii) fragmented mitochondrial morphology [33]; and (iii) low expression of parkin and selective vulnerability to proteasomal stress-triggered caspase activation [41,50].

In samples obtained from mice and PD patients, as well as from cultured cells, loss of PINK1 causes mitochondrial dysfunction and vulnerability to cell death.

Mitochondrial morphology: In mammalian cultured cells (with the exception of COS7 cells), PINK1 knockdown phenotype shows fragmented mitochondria [33,51]. In human neuroblastoma cells transduced with a PINK1 shRNA lentivirus, the activity of dynamin-related protein 1 (Drp1), which is controlled by phosphatase calcineurin, enhances the effects of PINK1 upon mitochondrial morphology [52]. In contrast, transgenic *Drosophila* with PINK1 promotes mitochondrial fission in dopaminergic neurons, whereas complete ablation of PINK1 leads to excessive fusion [53]. Fis1 (mitochondrial fission 1 protein) may act in-between PINK1 and Drp1 in controlling mitochondrial fission [53]. Heterozygous loss-of-function mutations of Drp1 are largely lethal in a *PINK1* or *parkin* mutant background. Conversely, the degeneration of flight muscle and mitochondrial morphological changes which result from mutations in *PINK1* and *parkin* are strongly suppressed by increasing the dosage of the Drp1 gene and by heterozygous loss-of-function mutations in OPA1 and Mfn2. In pseudopupil analyses, an eye phenotype associated with increased activity of the PINK1/parkin pathway is suppressed by perturbations that reduce mitochondrial fission but enhanced by perturbations that reduce mitochondrial fusion [54,55]. These results suggest that the PINK1/parkin pathway promotes mitochondrial fission, and that the loss of mitochondrial and tissue integrity in *PINK1* and *parkin* mutants is due to reduced mitochondrial fission in *Drosophila*. The cortical neurons of *PINK1*-deficient mice show reduced fission and increased aggregation of mitochondria only under stress [46]. Dopaminergic neuronal rat cells with a *PINK1* mutation (p.L347P) show mitochondrial fragmentation and dysfunction, which can be prevented by inhibitors of mitochondrial division [47,56].

There is controversy over whether PINK1 modulates mitochondrial fission or fusion. Fragmented mitochondria in *parkin* and/or *PINK1*-deficient *Drosophila* S2 cells are observed at day 2 after double-stranded RNA (dsRNA) treatment. At days 3 and 4 after dsRNA treatment, a dense network of fine thread-like mitochondria is observed. *PINK1*-deficient primary mouse hippocampal neurons show a decrease in the length of mitochondria and an increase in mitochondrial fragmentation. The mitochondrial phenotype observed in *parkin*- and *PINK1*-deficient cells can be rescued morphologically and functionally by increased expression of a dominant negative mutant of Drp1 [51]. Considering the discrepancy between cellular and fly models with low PINK1 expression, we might observe an acute manifestation of *parkin* or *PINK1* knockdown in cultured cells and the chronic phenotype influenced by compensatory effects in adult *Drosophila* (although the mitochondrial morphological change might be dependent upon cell lines). Otherwise, PINK1 might regulate and maintain a balance between fission and fusion depending upon certain conditions (e.g. phase stress).

Mitochondrial fission and fusion are highly regulated processes that are critical for the maintenance of mitochondria (especially in neurons). Imbalance of mitochondrial fission and fusion machineries has increasingly been linked to neurodegeneration [57]. Based on this concept, PINK1 has a crucial role in the pathogenesis of PD.

Mitophagy: Recent studies have provided new insights about the PINK1/parkin pathway. It has been reported that parkin is translocated to depolarized mitochondria and that the parkin-labeled mitochondria are subsequently eliminated by autophagy (mitophagy) [58]. Several studies on this pathway were subsequently reported. Endogenous PINK1 is not detected under basal conditions because it is rapidly degraded [16]. However, reduction of $\Delta\Psi m$ induced by carbonyl cyanide *m*-chlorophenylhydrazone (CCCP), a mitochondrial uncoupler, results in gradual accumulation of endogenous PINK1 (full-length form) on mitochondria [17,59]. Interestingly, clearance of CCCP results in immediate disappearance of the accumulated endogenous PINK1 in the presence and absence of cycloheximide (an inhibitor of protein biosynthesis) by interfering with the translocation step of protein synthesis.

Likewise, CCCP treatment does not alter PINK1 mRNA levels [17]. These results suggest that PINK1 is stabilized by reduced $\Delta\Psi m$ and subsequently accumulates on depolarized mitochondria. By contrast, parkin is not translocated to the mitochondria in *PINK1*-deficient CCCP-treated MEFs, and subsequent mitochondrial clearance is also completely blocked, indicating that PINK1 is indispensable for parkin translocation to depolarized mitochondria. Parkin E3 ligase activity is suppressed under basal conditions, although the activity is increased in mitochondria with low $\Delta\Psi m$. PINK1 accumulation induces recruitment of parkin to the depolarized mitochondria, and subsequently the mitochondria are eliminated by mitophagy. These processes are inhibited by pathogenic mutants of PINK1 or parkin [16,17,59]. Furthermore, elimination of parkin-labeled mitochondria is blocked in *Atg5*- or *Atg7*-deficient MEFs [58,59]. Moreover, MTS, kinase activity of PINK1, and the linker domain of parkin are indispensable for PINK1/parkin-mediated mitophagy [17,52,59].

In cells with normal $\Delta\Psi m$, expression of PINK1 on the outer mitochondrial membrane or overexpression of PINK1 induces translocation of parkin to the mitochondria [60,61]. Furthermore, valinomycin- and hydrogen peroxide (H_2O_2)-induced stress result in mitochondrial localization of parkin in skin fibroblasts of healthy controls but not in those of PD patients with PINK1 mutations (p.Q456X) [56,62]. Valinomycin, but not H_2O_2, reduces $\Delta\Psi m$. Taken together, it seems that PINK1 expression on the mitochondria, rather than low $\Delta\Psi m$, is indispensable for parkin translocation to the mitochondria.

The mitochondrial inner membrane rhomboid protease presenilin-associated rhomboid-like protein (PARL) mediates cleavage of PINK1 in the TMD in a $\Delta\Psi m$-dependent manner. In the absence of PARL, full-length PINK1 accumulates on the outer mitochondrial membrane, where it recruits parkin to the impaired mitochondria. Thus, the role of PARL in the PINK1/parkin pathway appears to include facilitating the rapid degradation of PINK1 by mediating the cleavage of PINK1 [19,20,63].

PINK1/parkin-mediated mitophagy involves the formation of linkage-specific polyubiquitin chains (K27 and K63) and requires the ubiquitin-autophagy adaptor p62/SQSTM1. VDAC1 is a mitochondrial target of parkin-dependent K27 ubiquitination, and VDAC1 ubiquitination in neuronal cells is dependent upon functional parkin. Because VDAC1 is a component of the mitochondrial permeability transition pore (mPTP), which is involved in apoptosis, a parkin-dependent, timely mitophagic clearance may prevent the release of pro-apoptotic factors from damaged mitochondria under physiological conditions [58,64]. By contrast, p62 is reported to be necessary for mitochondrial aggregation but not mitophagy, and mitochondrial-associated proteins other than VDAC1 and VDAC3 are K63-polyubiquitinated in a parkin-dependent manner [65,66]. Another candidate parkin substrate on the mitochondria is mitofusin (MFN), which is involved in mitochondrial fusion. *Drosophila* Marf (a fly MFN ortholog), which is localized on the outer surface of mitochondria, is ubiquitinated by parkin and accumulates in *parkin* mutants [67,68]. Mammalian cells contain two types of MFN: MFN1 and MFN2. Treatment of cultured cells with CCCP results in ubiquitination of MFN1 and MFN2 in a PINK1/parkin-dependent manner [63,69]. Moreover, parkin-ubiquitinated MFN1 and MFN2 are degraded by the proteasome. The hexametric AAA-type ATPase, p97, is required downstream of PINK1 and parkin to promote the proteasomal turnover of ubiquitinated MFN. Parkin-promoted MFN degradation prevents refusion of damaged mitochondria with healthy mitochondria [64,70]. Fission followed by selective fusion segregates dysfunctional mitochondria and permits their removal by autophagy [71]. These reports suggest that mitochondrial fission may be a key factor in PINK1/parkin-mediated mitophagy. However, there is controversy over the substrates of parkin, making further investigations necessary.

PINK1/parkin-mediated mitophagy model

Based on the collective results of the studies mentioned above, we propose the model illustrated in Figure 3 for PINK1/parkin-mediated mitophagy. PINK1 accumulated on the mitochondrial outer membrane due to the low $\Delta\Psi m$ or certain mitochondrial insults recruit parkin to the mitochondria. Parkin E3 ligase activity is subsequently activated and ubiquitinates MFN on the mitochondrial outer membrane. Ubiquitinated MFN assembles p97 and the complex is degraded by proteasome. Mitochondria lacking MFN, which cannot fuse with other healthy mitochondria, can be a target for mitophagy. The model advances our understanding of the pathogenic process of PD and the role of the direct associations between parkin and mitochondria, as well as between the PINK1/parkin pathway and autophagy. Mitochondrial dysfunction is also considered to be one of the main causes of the sporadic form of PD, and impaired autophagy leads to neurodegenerative diseases such as PD. However, to fully understand the molecular mechanisms of this pathway, further details are needed. For example, how does PINK1 recruit parkin to the damaged mitochondria? What is the mechanism responsible for parkin activation in the mitochondria? There is controversy over whether PINK1 phosphorylates parkin in this pathway [16,17,27,28,61,66]. PINK1 kinase activity is essential for parkin translocation to mitochondria [17,59]. Therefore, it is a feasible and attractive hypothesis that parkin is directly phosphorylated by PINK1. However, further investigations are needed.

Other candidate PINK1 substrates that recruit parkin or function as parkin receptors on the outer mitochondrial membrane also need to be investigated. In yeast, Atg32 (which has no known metazoan homolog) is identified as an outer mitochondrial membrane protein necessary for mitophagy [72,73], and contains a conserved WXXI/L/V motif for interaction with Atg8. Recent studies reported that another outer mitochondrial membrane protein, Nix (which has no yeast homolog and contains a WXXL-like motif), is crucial for PINK1/parkin-mediated mitophagy [68,74]. Does endogenous parkin contribute to mitophagy? Most reports on this pathway are conducted by overexpressing parkin. It remains unclear at this stage whether parkin deficiency or parkin partial knockdown down-regulates mitophagy. Furthermore, there is no information on whether $\Delta\Psi m$ of the brain is decreased in patients with

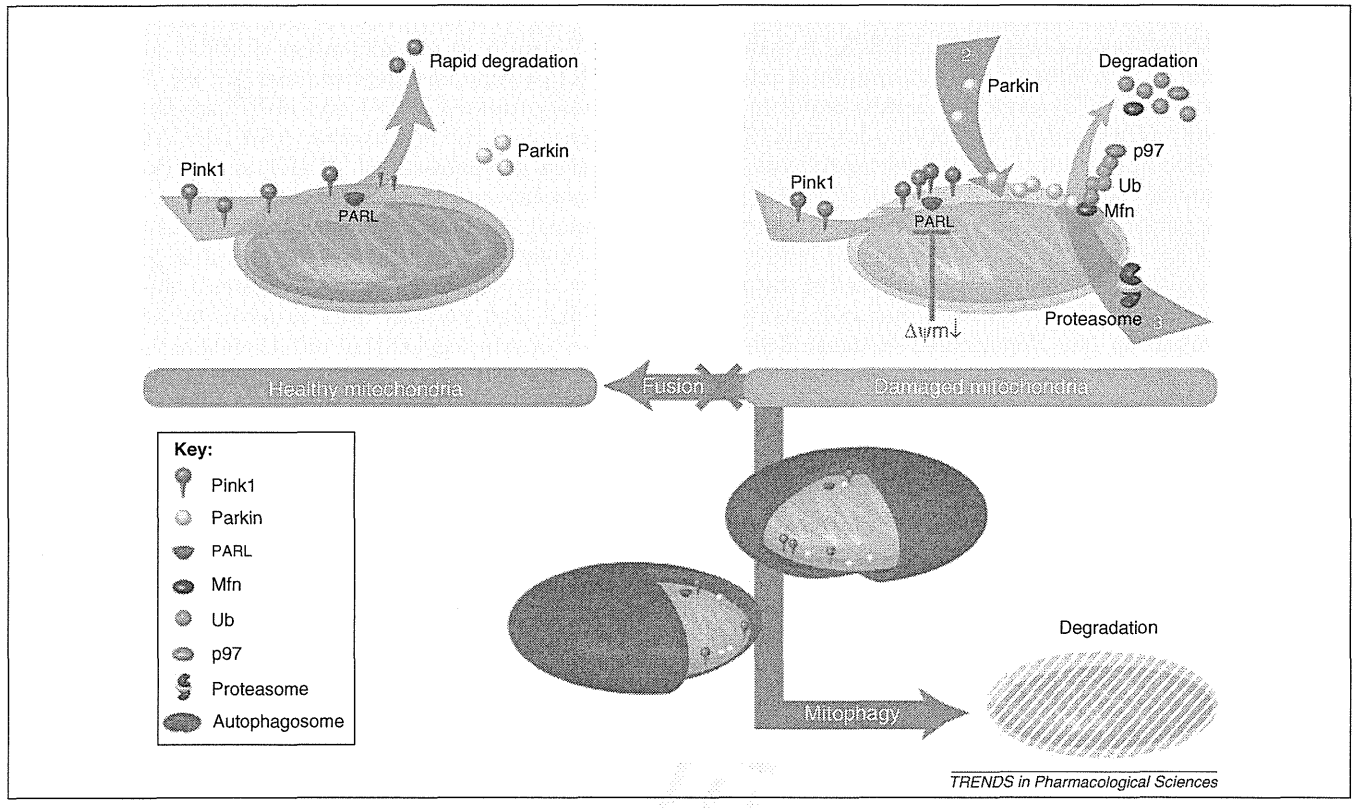

Figure 3. Proposed model of PINK1/parkin-mediated mitophagy. PINK1 on mitochondria is processed by PARL, which localizes in the mitochondrial inner membrane under basal conditions. The processed PINK1 is rapidly degraded by the proteasome. In the presence of a low membrane potential or certain insults to the mitochondria, PINK1 accumulates in the mitochondrial outer membrane. This results in translocation of parkin to the damaged mitochondria and subsequent activation of parkin-E3 ligase. Activated parkin ubiquitinates mitofusin (MFN) on the mitochondrial outer membrane. This leads to the assembly of p97 on ubiquitinated MFN and proteasomal degradation. Mitochondria lacking MFN cannot fuse with other healthy mitochondria and become a target for mitophagy.

sporadic PD. As mentioned above, *PINK1*-deficient mice and MEFs as well as PINK1 knockdown cells show decreased $\Delta\Psi m$. However, skin fibroblasts derived from neither the nonsense (p.Q456X) nor the missense (p.V170G) mutation show significantly low $\Delta\Psi m$ [75]. There is no model of CCCP-induced human parkinsonism, unlike with MPTP-and rotenone-induced parkinsonism. In this regard, there is no evidence for translocation of parkin to mitochondria in cells treated with MPTP or rotenone. CCCP treatment does not reflect a human physiological condition. Therefore, there is a limitation in discussing the pathogenesis of PD using models based on CCCP treatment.

Is there any association between PINK1/parkin-mediated mitophagy and α-synuclein? As discussed above, α-synuclein is a major component of Lewy bodies (the hallmark of sporadic PD) and is considered to be a key protein in the pathogenesis of sporadic PD. There is no direct association between PINK1/parkin-mediated mitophagy and α-synuclein, although wild-type and mutants of α-synuclein are degraded by chaperone-mediated autophagy and macroautophagy, respectively [76,77]. Studies demonstrated that α-synuclein inhibits autophagy [71,78], and that inhibition of mitochondrial fusion by α-synuclein is rescued by PINK1 and parkin [72,73,79]. To develop a novel therapeutic strategy for sporadic PD as well as *PINK1*- and *parkin*-linked PD, it is necessary to investigate the relationship between aggregation of α-synuclein and dysfunction of PINK1/parkin-mediated mitophagy.

Concluding remarks

PD is a progressive neurodegenerative disease for which the frequency increases with age. As 'developing nations' face rapidly aging populations, the prevalence of PD is expected to rise. PD patients in the advanced stage require great support from families and the medical community. However, curative therapies to suppress the progression are lacking. Therefore, it is important to elucidate the pathogenesis and establish novel and rational treatments. PINK1 provides valuable clues regarding the molecular pathogenesis of PD because the pathomechanism for sporadic PD probably has certain common pathways with that of *PINK1*-linked PD. Based on the available information on PINK1, we propose the model shown in Figure 2 for the mechanisms involved in the development of *PINK1*-linked PD. PINK1 mainly protects the mitochondria via mitophagy with parkin, and may subsequently suppress neuronal cell death due to reduced dopamine release. However, PINK1 may have a cytoprotective function by activating Akt in the cytoplasm. We expect that a compound which inhibits this pathway could be established as a novel treatment for not only *PINK1*-linked PD but also sporadic PD. In particular, PINK1/parkin-mediated mitophagy (i.e. mitochondrial quality control via autophagic machinery that includes the combination of PINK1 and parkin) could be viewed as the foundation for the design of novel therapies for PD, although several issues remain unresolved. If we could determine the precise mechanism of mitophagy which eliminates abnormal mitochondria, we

might regulate the clearance of deleterious mitochondria with new chemicals which target this pathway to maintain cell integrity and subsequently suppress cell death. However, further studies are required to elucidate the exact pathomechanism and develop effective therapies for hereditary PD and sporadic PD.

Acknowledgements

Q1 The authors thank Ms. Ayako Yamaguchi (JOKER) for preparation of the illustrations. The study was supported by the Takeda Scientific Foundation (Drs. Sato and Saiki) and (JSPS) Kakenhi (Dr. Hattori).

References

1 de Lau, L.M. and Breteler, M.M. (2006) Epidemiology of Parkinson's disease. *Lancet Neurol.* 5, 525–535
2 Schapira, A.H. (2008) Mitochondria in the aetiology and pathogenesis of Parkinson's disease. *Lancet Neurol.* 7, 97–109
3 Hatano, T. *et al.* (2009) Pathogenesis of familial Parkinson's disease: new insights based on monogenic forms of Parkinson's disease. *J. Neurochem.* 111, 1075–1093
4 Petit, A. *et al.* (2005) Wild-type PINK1 prevents basal and induced neuronal apoptosis, a protective effect abrogated by Parkinson disease-related mutations. *J. Biol. Chem.* 280, 34025–34032
5 Pridgeon, J.W. *et al.* (2007) PINK1 protects against oxidative stress by phosphorylating mitochondrial chaperone TRAP1. *PLoS Biol.* 5, e172
6 Plun-Favreau, H. *et al.* (2007) The mitochondrial protease HtrA2 is regulated by Parkinson's disease-associated kinase PINK1. *Nat. Cell Biol.* 9, 1243–1252
7 Hatano, Y. *et al.* (2004) PARK6-linked autosomal recessive early-onset parkinsonism in Asian populations. *Neurology* 63, 1482–1485
8 Ibanez, P. *et al.* (2006) Mutational analysis of the PINK1 gene in early-onset parkinsonism in Europe and North Africa. *Brain* 129, 686–694
9 Kumazawa, R. *et al.* (2008) Mutation analysis of the PINK1 gene in 391 patients with Parkinson disease. *Arch. Neurol.* 65, 802–808
10 Samaranch, L. *et al.* (2010) PINK1-linked parkinsonism is associated with Lewy body pathology. *Brain* 133, 1128–1142
11 Hayashi, S. *et al.* (2000) An autopsy case of autosomal-recessive juvenile parkinsonism with a homozygous exon 4 deletion in the parkin gene. *Mov. Disord.* 15, 884–888
12 van de Warrenburg, B.P. *et al.* (2001) Clinical and pathologic abnormalities in a family with parkinsonism and parkin gene mutations. *Neurology* 56, 555–557
13 Valente, E.M. *et al.* (2004) Hereditary early-onset Parkinson's disease caused by mutations in PINK1. *Science* 304, 1158–1160
14 Zhou, C. *et al.* (2008) The kinase domain of mitochondrial PINK1 faces the cytoplasm. *Proc. Natl. Acad. Sci. U.S.A.* 105, 12022–12027
15 Beilina, A. *et al.* (2005) Mutations in PTEN-induced putative kinase 1 associated with recessive parkinsonism have differential effects on protein stability. *Proc. Natl. Acad. Sci. U.S.A.* 102, 5703–5708
16 Lin, W. and Kang, U.J. (2008) Characterization of PINK1 processing, stability, and subcellular localization. *J. Neurochem.* 106, 464–474
17 Narendra, D.P. *et al.* (2010) PINK1 is selectively stabilized on impaired mitochondria to activate Parkin. *PLoS Biol.* 8, e1000298
18 Silvestri, L. *et al.* (2005) Mitochondrial import and enzymatic activity of PINK1 mutants associated to recessive parkinsonism. *Hum. Mol. Genet.* 14, 3477–3492
19 Jin, S.M. *et al.* (2010) Mitochondrial membrane potential regulates PINK1 import and proteolytic destabilization by PARL. *J. Cell Biol.* 191, 933–942
20 Deas, E. *et al.* (2011) PINK1 cleavage at position A103 by the mitochondrial protease PARL. *Hum. Mol. Genet.* 20, 867–879
21 Hatano, Y. *et al.* (2004) Novel PINK1 mutations in early-onset parkinsonism. *Annu. Neurol.* 56, 424–427
22 Klein, C. and Schlossmacher, M.G. (2007) Parkinson disease, 10 years after its genetic revolution: multiple clues to a complex disorder. *Neurology* 69, 2093–2104
23 Li, Y. *et al.* (2005) Clinicogenetic study of PINK1 mutations in autosomal recessive early-onset parkinsonism. *Neurology* 64, 1955–1957
24 Klein, C. *et al.* (2007) Deciphering the role of heterozygous mutations in genes associated with parkinsonism. *Lancet Neurol.* 6, 652–662
25 Sim, C.H. *et al.* (2006) C-terminal truncation and Parkinson's disease-associated mutations down-regulate the protein serine/threonine kinase activity of PTEN-induced kinase-1. *Hum. Mol. Genet.* 15, 3251–3262
26 Rohe, C.F. *et al.* (2004) Homozygous PINK1 C-terminus mutation causing early-onset parkinsonism. *Annu. Neurol.* 56, 427–431
27 Kim, Y. *et al.* (2008) PINK1 controls mitochondrial localization of Parkin through direct phosphorylation. *Biochem. Biophys. Res. Commun.* 377, 975–980
28 Sha, D. *et al.* (2010) Phosphorylation of parkin by Parkinson disease-linked kinase PINK1 activates parkin E3 ligase function and NF-kappaB signaling. *Hum. Mol. Genet.* 19, 352–363
29 Murata, H. *et al.* (2011) A New Cytosolic Pathway from a Parkinson Disease-associated Kinase, BRPK/PINK1: ACTIVATION OF AKT VIA MTORC2. *J. Biol. Chem.* 286, 7182–7189
30 Park, J. *et al.* (2006) Mitochondrial dysfunction in Drosophila PINK1 mutants is complemented by parkin. *Nature* 441, 1157–1161
31 Clark, I.E. *et al.* (2006) Drosophila pink1 is required for mitochondrial function and interacts genetically with parkin. *Nature* 441, 1162–1166
32 Yun, J. *et al.* (2008) Loss-of-function analysis suggests that Omi/HtrA2 is not an essential component of the PINK1/PARKIN pathway in vivo. *J. Neurosci.* 28, 14500–14510
33 Exner, N. *et al.* (2007) Loss-of-function of human PINK1 results in mitochondrial pathology and can be rescued by parkin. *J. Neurosci.* 27, 12413–12418
34 Shiba, K. *et al.* (2009) Parkin stabilizes PINK1 through direct interaction. *Biochem. Biophys. Res. Commun.* 383, 331–335
35 Xiong, H. *et al.* (2009) Parkin, PINK1, and DJ-1 form a ubiquitin E3 ligase complex promoting unfolded protein degradation. *J. Clin. Invest.* 119, 650–660
36 Hao, L.Y. *et al.* (2010) DJ-1 is critical for mitochondrial function and rescues PINK1 loss of function. *Proc. Natl. Acad. Sci. U.S.A.* 107, 9747–9752
37 Thomas, K.J. *et al.* (2011) DJ-1 acts in parallel to the PINK1/parkin pathway to control mitochondrial function and autophagy. *Hum. Mol. Genet.* 20, 40–50
38 Liu, W. *et al.* (2009) PINK1 defect causes mitochondrial dysfunction, proteasomal deficit and alpha-synuclein aggregation in cell culture models of Parkinson's disease. *PLoS ONE* 4, e4597
39 Samann, J. *et al.* (2009) Caenorhabditits elegans LRK-1 and PINK-1 act antagonistically in stress response and neurite outgrowth. *J. Biol. Chem.* 284, 16482–16491
40 Venderova, K. *et al.* (2009) Leucine-rich repeat kinase 2 interacts with Parkin, DJ-1 and PINK-1 in a Drosophila melanogaster model of Parkinson's disease. *Hum. Mol. Genet.* 18, 4390–4404
41 Haque, M.E. *et al.* (2008) Cytoplasmic Pink1 activity protects neurons from dopaminergic neurotoxin MPTP. *Proc. Natl. Acad. Sci. U.S.A.* 105, 1716–1721
42 Deng, H. *et al.* (2005) Small interfering RNA targeting the PINK1 induces apoptosis in dopaminergic cells SH-SY5Y. *Biochem. Biophys. Res. Commun.* 337, 1133–1138
43 Morais, V.A. *et al.* (2009) Parkinson's disease mutations in PINK1 result in decreased Complex I activity and deficient synaptic function. *EMBO Mol. Med.* 1, 99–111
44 Kitada, T. *et al.* (2007) Impaired dopamine release and synaptic plasticity in the striatum of PINK1-deficient mice. *Proc. Natl. Acad. Sci. U.S.A.* 104, 11441–11446
45 Gautier, C.A. *et al.* (2008) Loss of PINK1 causes mitochondrial functional defects and increased sensitivity to oxidative stress. *Proc. Natl. Acad. Sci. U.S.A.* 105, 11364–11369
46 Gispert, S. *et al.* (2009) Parkinson phenotype in aged PINK1-deficient mice is accompanied by progressive mitochondrial dysfunction in absence of neurodegeneration. *PLoS ONE* 4, e5777
47 Gandhi, S. *et al.* (2009) PINK1-associated Parkinson's disease is caused by neuronal vulnerability to calcium-induced cell death. *Mol. Cell* 33, 627–638
48 Amo, T. *et al.* (2011) Mitochondrial membrane potential decrease caused by loss of PINK1 is not due to proton leak, but to respiratory chain defects. *Neurobiol. Dis.* 41, 111–118
49 Hoepken, H.H. *et al.* (2007) Mitochondrial dysfunction, peroxidation damage and changes in glutathione metabolism in PARK6. *Neurobiol. Dis.* 25, 401–411

50 Klinkenberg, M. *et al.* (2010) Enhanced vulnerability of PARK6 patient skin fibroblasts to apoptosis induced by proteasomal stress. *Neuroscience* 166, 422–434
51 Lutz, A.K. *et al.* (2009) Loss of parkin or PINK1 function increases Drp1-dependent mitochondrial fragmentation. *J. Biol. Chem.* 284, 22938–22951
52 Sandebring, A. *et al.* (2009) Mitochondrial alterations in PINK1 deficient cells are influenced by calcineurin-dependent dephosphorylation of dynamin-related protein 1. *PLoS ONE* 4, e5701
53 Yang, Y. *et al.* (2008) Pink1 regulates mitochondrial dynamics through interaction with the fission/fusion machinery. *Proc. Natl. Acad. Sci. U.S.A.* 105, 7070–7075
54 Deng, H. *et al.* (2008) The Parkinson's disease genes pink1 and parkin promote mitochondrial fission and/or inhibit fusion in Drosophila. *Proc. Natl. Acad. Sci. U.S.A.* 105, 14503–14508
55 Poole, A.C. *et al.* (2008) The PINK1/Parkin pathway regulates mitochondrial morphology. *Proc. Natl. Acad. Sci. U.S.A.* 105, 1638–1643
56 Cui, M. *et al.* (2010) Perturbations in mitochondrial dynamics induced by human mutant PINK1 can be rescued by the mitochondrial division inhibitor mdivi-1. *J. Biol. Chem.* 285, 11740–11752
57 Chan, D.C. (2006) Mitochondria: dynamic organelles in disease, aging, and development. *Cell* 125, 1241–1252
58 Narendra, D. *et al.* (2008) Parkin is recruited selectively to impaired mitochondria and promotes their autophagy. *J. Cell Biol.* 183, 795–803
59 Matsuda, N. *et al.* (2010) PINK1 stabilized by mitochondrial depolarization recruits Parkin to damaged mitochondria and activates latent Parkin for mitophagy. *J. Cell Biol.* 189, 211–221
60 Kawajiri, S. *et al.* (2010) PINK1 is recruited to mitochondria with parkin and associates with LC3 in mitophagy. *FEBS Lett.* 584, 1073–1079
61 Vives-Bauza, C. *et al.* (2010) PINK1-dependent recruitment of Parkin to mitochondria in mitophagy. *Proc. Natl. Acad. Sci. U.S.A.* 107, 378–383
62 Rakovic, A. *et al.* (2010) Effect of endogenous mutant and wild-type PINK1 on Parkin in fibroblasts from Parkinson disease patients. *Hum. Mol. Genet.* 19, 3124–3137
63 Whitworth, A.J. *et al.* (2008) Rhomboid-7 and HtrA2/Omi act in a common pathway with the Parkinson's disease factors Pink1 and Parkin. *Dis. Model. Mech.* 1, 168–174 discussion 173
64 Geisler, S. *et al.* (2010) PINK1/Parkin-mediated mitophagy is dependent on VDAC1 and p62/SQSTM1. *Nat. Cell Biol.* 12, 119–131
65 Okatsu, K. *et al.* (2010) p62/SQSTM1 cooperates with Parkin for perinuclear clustering of depolarized mitochondria. *Genes Cells* 15, 887–900
66 Narendra, D. *et al.* (2010) p62/SQSTM1 is required for Parkin-induced mitochondrial clustering but not mitophagy; VDAC1 is dispensable for both. *Autophagy* 6, 1090–1106
67 Ziviani, E. *et al.* (2010) Drosophila parkin requires PINK1 for mitochondrial translocation and ubiquitinates mitofusin. *Proc. Natl. Acad. Sci. U.S.A.* 107, 5018–5023
68 Poole, A.C. *et al.* (2010) The mitochondrial fusion-promoting factor mitofusin is a substrate of the PINK1/parkin pathway. *PLoS ONE* 5, e10054
69 Gegg, M.E. *et al.* (2010) Mitofusin 1 and mitofusin 2 are ubiquitinated in a PINK1/parkin-dependent manner upon induction of mitophagy. *Hum. Mol. Genet.* 19, 4861–4870
70 Tanaka, A. *et al.* (2010) Proteasome and p97 mediate mitophagy and degradation of mitofusins induced by Parkin. *J. Cell Biol.* 191, 1367–1380
71 Twig, G. *et al.* (2008) Fission and selective fusion govern mitochondrial segregation and elimination by autophagy. *EMBO J.* 27, 433–446
72 Kanki, T. *et al.* (2009) Atg32 is a mitochondrial protein that confers selectivity during mitophagy. *Dev. Cell* 17, 98–109
73 Okamoto, K. *et al.* (2009) Mitochondria-anchored receptor Atg32 mediates degradation of mitochondria via selective autophagy. *Dev. Cell* 17, 87–97
74 Ding, W.X. *et al.* (2010) Nix is critical to two distinct phases of mitophagy, reactive oxygen species-mediated autophagy induction and Parkin-ubiquitin-p62-mediated mitochondrial priming. *J. Biol. Chem.* 285, 27879–27890
75 Grunewald, A. *et al.* (2009) Differential effects of PINK1 nonsense and missense mutations on mitochondrial function and morphology. *Exp. Neurol.* 219, 266–273
76 Cuervo, A.M. *et al.* (2004) Impaired degradation of mutant alpha-synuclein by chaperone-mediated autophagy. *Science* 305, 1292–1295
77 Webb, J.L. *et al.* (2003) Alpha-Synuclein is degraded by both autophagy and the proteasome. *J. Biol. Chem.* 278, 25009–25013
78 Winslow, A.R. *et al.* (2010) alpha-Synuclein impairs macroautophagy: implications for Parkinson's disease. *J. Cell Biol.* 190, 1023–1037
79 Kamp, F. *et al.* (2010) Inhibition of mitochondrial fusion by alpha-synuclein is rescued by PINK1, Parkin and DJ-1. *EMBO J.* 29, 3571–3589

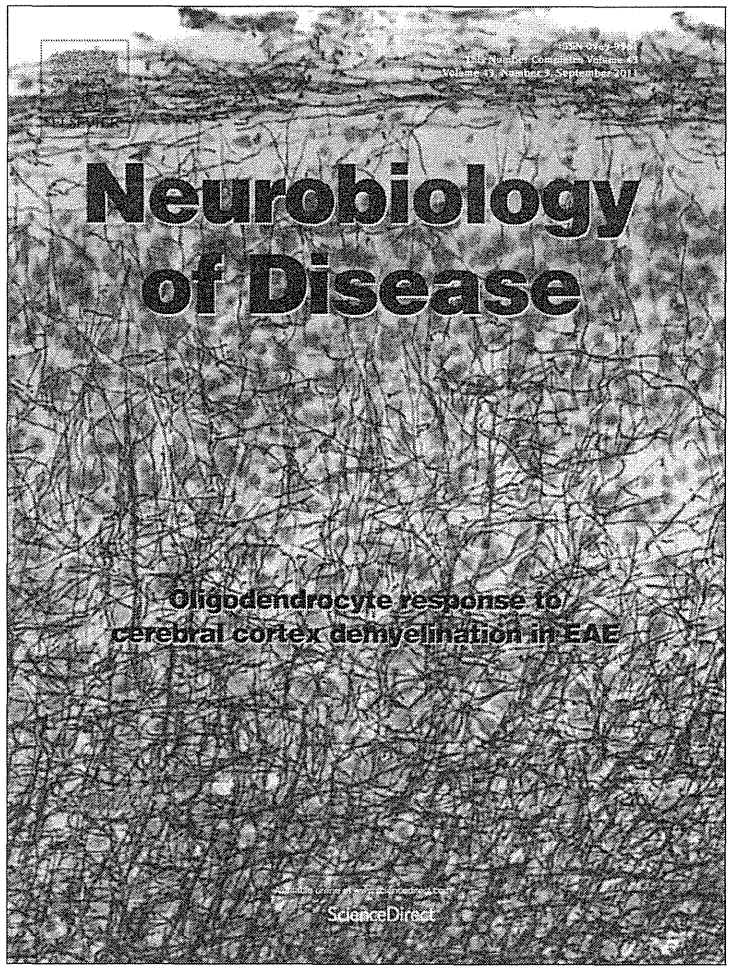

Neurobiology of Disease 43 (2011) 651–662

Contents lists available at ScienceDirect

Neurobiology of Disease

journal homepage: www.elsevier.com/locate/ynbdi

DJ-1 associates with synaptic membranes

Yukiko Usami [a], Taku Hatano [a], Satoshi Imai [b,1], Shin-ichiro Kubo [a], Shigeto Sato [a], Shinji Saiki [a], Yoichiro Fujioka [c], Yusuke Ohba [c], Fumiaki Sato [b,2], Manabu Funayama [a,b], Hiroto Eguchi [a], Kaori Shiba [b], Hiroyoshi Ariga [d], Jie Shen [e], Nobutaka Hattori [a,b,*]

[a] Department of Neurology, Juntendo University School of Medicine, Japan
[b] Research Institute for Diseases of Old Age, Graduate School of Medicine, Juntendo University, Japan
[c] Laboratory of Pathophysiology and Signal Transduction, Hokkaido University Graduate School of Medicine, Japan
[d] Graduate School of Pharmaceutical Sciences, Hokkaido University, Japan
[e] Center for Neurologic Diseases, Brigham and Women's Hospital Program in Neuroscience, Harvard Medical School, USA

ARTICLE INFO

Article history:
Received 6 February 2011
Revised 30 April 2011
Accepted 20 May 2011
Available online 30 May 2011

Keywords:
DJ-1
Parkinson's disease
Localization
Synaptic vesicles
Synaptophysin
VAMP2
Rab3A

ABSTRACT

Parkinson's disease (PD) is a neurodegenerative disorder caused by loss of dopaminergic neurons. Although many reports have suggested that genetic factors are implicated in the pathogenesis of PD, molecular mechanisms underlying selective dopaminergic neuronal degeneration remain unknown. *DJ-1* is a causative gene for autosomal recessive form of *PARK7*-linked early-onset PD. A number of studies have demonstrated that exogenous DJ-1 localizes within mitochondria and the cytosol, and functions as a molecular chaperon, as a transcriptional regulator, and as a cell protective factor against oxidative stress. However, the precise subcellular localization and function of endogenous DJ-1 are not well known. The mechanisms by which mutations in DJ-1 contributes to neuronal degeneration also remain poorly understood. Here we show by immunocytochemistry that DJ-1 distributes to the cytosol and membranous structures in a punctate appearance in cultured cells and in primary neurons obtained from mouse brain. Interestingly, DJ-1 colocalizes with the Golgi apparatus proteins GM130 and the synaptic vesicle proteins such as synaptophysin and Rab3A. Förster resonance energy transfer analysis revealed that a small portion of DJ-1 interacts with synaptophysin in living cells. Although the wild-type DJ-1 protein directly associates with membranes without an intermediary protein, the pathogenic L166P mutation of DJ-1 exhibits less binding to synaptic vesicles. These results indicate that DJ-1 associates with membranous organelles including synaptic membranes to exhibit its normal function.

Introduction

Parkinson's disease (PD) is the second most common neurodegenerative disorder next to Alzheimer's disease and is characterized by motor symptoms as cardinal features such as resting tremor, rigidity, bradykinesia and postural instability. Pathological hallmarks of PD include marked cell loss of dopaminergic neurons in the substantia nigra pars compacta which causes dopamine depletion in the striatum and the presence of intracytoplasmic inclusions known as Lewy bodies in the remaining neurons (Fearnley and Lees, 1991). Although most of the PD cases are sporadic, approximately 5% of PD patients have clear familial etiology. Thus, the presence of monogenic forms of familial PD tells us that genetic factors contribute to the pathogenesis of PD. Indeed, heterozygous and homozygous mutations in one of the responsible genes have been reported in sporadic cases, suggesting that genetic factors are implicated in the pathogenesis of PD. Until now, 9 genes for familial PD have been reported, and these include *α-synuclein*, *parkin*, *UCH-L*, *PINK-1*, *DJ-1*, *LRRK2*, *ATP13A2*, *PLA2G6*, and *FBXO7* (Hatano et al., 2009).

Previous reports have suggested that DJ-1 functions as a molecular chaperon (Lee et al., 2003), a transcriptional regulator (Kim et al., 2005; Niki et al., 2003; Shinbo et al., 2005; Takahashi et al., 2001), and as a cell protective factor against oxidative stress (Canet-Aviles et al., 2004; Taira et al., 2004b; Yokota et al., 2003). The localization of DJ-1 has been shown to be in mitochondria, cytosol, nucleus, and microsomes (endoplasmic reticulum (ER) and Golgi) (Bonifati et al., 2003; Canet-Aviles et al., 2004; Miller et al., 2003; Taira et al., 2004a). However, most studies have been performed by exogenous DJ-1 using overexpression systems. On the other hand, endogenous DJ-1 is present in synaptic terminals, in both axons and dendrites, as well as

Abbreviations: PD, Parkinson's disease; FRET, Förster resonance energy transfer; WT, wild type; ER, endoplasmic reticulum; KO, knockout; RT, room temperature; PBS, phosphate-buffer saline; FBS, fetal bovine serum; BSA, bovine serum albumin; Tfn-R, transferrin receptor; IR, immunoreactivity; HB, homogenizing buffer.

* Corresponding author at: Department of Neurology, Juntendo University School of Medicine, 2-1-1 Hongo, Bunkyo-ku, Tokyo 113-8421, Japan. Fax: +81 3 5800 0547.
E-mail address: nhattori@juntendo.ac.jp (N. Hattori).
[1] Present affiliation: Department of Toxicology, School of Pharmacy and Pharmaceutical Sciences, Hoshi University, Japan.
[2] Present affiliation: Department of Clinical Chemistry, School of Pharmacy and Pharmaceutical Sciences, Hoshi University, Japan.

Available online on ScienceDirect (www.sciencedirect.com).

0969-9961/$ – see front matter © 2011 Elsevier Inc. All rights reserved.
doi:10.1016/j.nbd.2011.05.014

in mitochondria (Olzmann et al., 2007; Zhang et al., 2005). However, the precise function and dynamics of DJ-1 related to vesicular trafficking remain unclear. In the present study, we demonstrate the association of endogenous DJ-1 with membranous organelles and the molecular interaction of recombinant DJ-1 protein with membranes in cultured cells. In addition, we examine whether pathogenic mutations found in *PARK7*-linked early onset PD patients may be affected by binding activities of DJ-1.

Materials and methods

Antibodies and recombinant proteins

Mouse monoclonal antibody (M043-3, Clone 3E8) and rabbit polyclonal antibody (NB300-270) for DJ-1 were obtained from Medical & Biological Laboratories Co. (MBL, Nagoya, Japan) and Novus Biologicals, Inc. (Littleton, CO), respectively. Rabbit polyclonal antibodies to Rab3A (sc-308), Rab4A (sc-312), Rab5B (sc-598), and Tom20 (sc-11415) were purchased from Santa Cruz Biotechnology (Santa Cruz, CA), and Rab7B (R4779) was obtained from Sigma (St. Louis, MO). Mouse monoclonal antibodies to synaptophysin were purchased from Chemicon International, Inc. (MAB5258, Temecula, CA) (used for immunoblotting) and Progen Biotechnik (61012, Heidelberg, Germany) (used for immunocytochemistry). Synaptotagmin (610434) and NMDAR1 (556308) were obtained from BD Biosciences Pharmingen (San Diego, CA). Other primary antibodies were Rab3A (107111, Synaptic Systems, Gottingen, Germany), anti-human transferrin receptor (13-6800, Zymed Laboratories, South San Francisco, CA), Parkin (#4211) and Calnexin (#2679S) (Cell Signaling, Danvers, MA), VAMP2 (NB300-595, Novus Biologicals, Inc.), BIP2 (ab21685, Abcam, Cambridge, MA), Hsp70 (610608, BD Transduction Laboratories), Mito Tracker Red CMXRos (M-7512, Molecular Probes), and total OXPHOS rodent WB antibody cocktail (MS604; MitoSciences, Eugene, Oregon). Secondary antibodies conjugated to horseradish peroxidase were purchased from GE HealthCare Bio-Sciences (Piscataway, USA). From Invitrogen Molecular Probes, 488 and 546 conjugated secondary antibodies were purchased. The vectors encoding GST-tagged WT and mutants DJ-1 (M26I, A104T, D149A, and L166P) were kindly provided by Hiroyoshi Ariga (Laboratory of Pharmaceutical Science, Hokkaido University).

Experimental animals (DJ-1 KO mice)

The DJ-1 KO mice (F2) were a kind gift from The Laboratory of Pharmaceutical Science, Hokkaido University. The DJ-1 KO mice were generated at the Center for Neurologic Diseases, Brigham and Women's Hospital Program in Neuroscience, Harvard Medical School (Goldberg et al., 2005). F2 progeny were backcrossed for five generations to C57BL/6 mice, and heterozygotes were intercrossed to generate homozygous mice for the targeted *DJ-1* allele. For the experiments, C57BL/6J mice and DJ-1 KO mice were used at 7 to 9 weeks of age. All animal experiments were carried out in accordance with the Ethics Review Committee for Animal Experimentation of Juntendo University School of Medicine.

Cell culture and transfection

SH-SY5Y cells and HeLa cells were grown in Dulbecco's modified Eagle's medium (D-MEM, Sigma) with 10% fetal bovine serum (FBS; Sigma) and 1% penicillin–streptomycin (PS; Invitrogen). SH-SY5Y cell culture medium was supplemented with 1% non-essential amino acid, 1% sodium pyruvate, and 1% L-glutamate (Invitrogen). The cells were cultured at 37 °C and 5% CO_2. PC12 cells were grown in D-MEM with 5% FBS and 10% horse serum. Primary cortical neurons containing glia cells were prepared from E15.5 C57BL/6J mice and cultured for growth on Fisher-brand cover glass (Fisher Scientific, Pittsburgh, USA) in starting medium (F12 and Minimum Essential Medium with 10% FBS, 1% PS, and 0.001% insulin) for 3 days, and incubated sequentially for 5 days with 0.5 μM Ara-C (Sigma) in maintenance medium (F12 and Minimum Essential Medium with 5% calf serum, 5% horse serum, 1% PS, and 0.001% insulin). HeLa cells were transfected with expression vectors for FLAG-DJ-1 WT, M26I, A104T, D149A, or L166P by using FuGENE HD Transfection Reagent (Roche). After 24 h, immunocytochemistry was performed on the cells.

Immunocytochemistry

Cells were fixed for 10 min in 4% paraformaldehyde and 0.5% sucrose in phosphate-buffered saline (PBS). The cells were permeabilized with PBS containing 0.2% Triton X-100 (Sigma) for 5 min at RT. For blocking, 1× BlockAce (Yukijirushi Co., Osaka, Japan) was used for SH-SY5Y cells, and 10% FBS and 1% bovine serum albumin (BSA) in PBS (primary cortical neurons from mice) was used for primary cortical neurons for 30 min. Cells were incubated overnight with primary antibodies at 4 °C. The cells were washed 3 times with PBS and were incubated at RT for 1 h with secondary antibodies. After the cells were washed 3 times with PBS, the slides were mounted with Vectashield (Vector Laboratories, Burlingame, CA) and analyzed using a Leica confocal microscopy.

Preparation of synaptosome fractions from mouse brain

Synaptic vesicles were prepared as described previously (Hatano et al., 2007; Hell, 1998), with some modification. Briefly, whole brains from 3 mice (C57BL/6J) at 7 to 9 weeks of age were placed into 8 ml ice-cold synaptosomal homogenizing buffer (HB) (0.32 M sucrose, 4 mM HEPES–NaOH, pH 7.4 with EDTA-free protease inhibitor cocktail Complete Mini, EDTA free). The tissues were homogenized using a glass-Teflon homogenizer (10 up and down strokes, 830 rpm). The homogenized brain sample was centrifuged at 1000*g* for 10 min at 4 °C. After the supernatant (S1-1) was removed, the pellet was re-suspended in 5 ml HB and was homogenized and centrifuged at the same speed. The supernatant (S1-2) was removed, and the pellet was resuspended in 3 ml HB, and was homogenized and centrifuged in the same manner. The pellet was considered the P1 fraction, while the supernatant (mixed with S1-1, S1-2, and S1-3) was centrifuged at 12,000*g* for 15 min at 4 °C. The supernatant (S2) was removed and the pellet (P2) was resuspended with HB, and then centrifuged for 15 min at 13,000*g* at 4 °C. After removal of the supernatant (S2′), the pellet (P2′) was collected as the crude synaptosome fraction. P2′ was subsequently re-suspended with HB to a final volume of 1 ml. The P2′ fraction was suspended with 4 ml of ice cold water in the EDTA-free protease inhibitor cocktail. The samples were homogenized by 6 up and down strokes of the glass-Teflon homogenizer at 830 rpm and mixed with 39 μl 1 M HEPES, pH 7.4, then centrifuged for 20 min at 33,000*g* at 4 °C. The lysate pellet was considered the LP1 fraction, and the supernatant (LS1) was centrifuged for 2 h at 260,000*g* at 4 °C. After the supernatant (LS2) was removed, the pellet (LP2) was resuspended with 300 μl of HB. To loosen the pellet, samples were extruded consecutively through a 23-gauge and a 26-gauge hypodermic needle attached to a 1 ml syringe. The concentration of protein in each of the fractions was calculated using the BCA protein assay kit (Pierce, Rockford, IL). Finally, the same amounts of proteins from each fraction were analyzed by SDS–PAGE followed by immunoblotting.

Sucrose gradients of LS1 fraction from mouse brain

The LS1 fraction was layered on top of a linear sucrose density gradient ranging from 0.2 to 2.0 M sucrose dissolved in HEPES buffer (pH 7.4), and ultra-centrifuged at 465,000*g* for 13 h at 4 °C. Each of the fractions (0.5 ml) was collected from the top of the gradient, and equal volumes of each fraction were subjected to SDS–PAGE followed by immunoblotting.

Preparation of magnetic beads cross-linked with antibodies

For the following experiments of immunoisolation and immunoprecipitation, the DJ-1 polyclonal antibody and the synaptophysin antibody, and the normal rabbit IgG and the normal mouse IgG as control, were cross-linked to protein G-coated magnetic beads (Dynabeads Invitrogen). The beads were washed 3 times with citrate buffer, and then 50 μl of magnetic bead slurry was combined with 50 μg of each antibody by rotating for 1 h at RT. The antibody-bound beads were washed 3 times with 0.2 M sodium borate buffer (pH 9.0), and then resuspended in 0.2 M sodium borate buffer containing dimethyl pimelimidate (Pierce Biotechnology). After reacting by rotating the samples for 1 h at RT, the supernatants were removed and the Dynabead pellets were washed 3 times with 0.2 M triethanolamine buffer (pH 8.0). The washed beads were suspended with 0.2 M triethanolamine buffer containing 50 mM glycine, and were reacted for 2 h at RT. The supernatant was removed and the beads were washed 3 times with PBS, stored at 4 °C with PBS containing 0.05% Tween 20, and used within 1 week of the reactions.

Immunoisolation and immunoprecipitation of LS1 fraction containing synaptic vesicles from the mouse brain

Immunoisolation: beads cross-linked with DJ-1 antibody and synaptophysin antibody, or beads cross-linked with normal rabbit IgG and normal mouse IgG were washed 6 times with PBS and were blocked for 1 h at RT using PBS containing 10% BSA as nonspecific competitor, followed by washing in PBS 3 times. In addition, each of the 1 ml LS1 fraction samples were immunoisolated with 37.5 μl of the beads cross-linked with antibody for a total of 12 h at 4 °C after blocking non-specific sites by rotating with the beads with the cross-linked normal rabbit IgG, or normal mouse IgG for 1 h at 4 °C. The pellets and supernatants were subjected to SDS–PAGE followed by immunoblotting using antibodies against the indicated proteins.

Immunoprecipitation: beads cross-linked with the antibodies, the same as in the immunoisolation protocol, were blocked using PBS containing 10% BSA for 1 h at RT. LS1 fractions (900 μl) were dissolved in 100 μl of 10× RIPA buffer (final concentration: 140 mM KCl, 20 mM HEPES–KOH (pH 7.3), 2 mM EDTA, protease inhibitors, and 1% Triton X-100), and then the samples were blocked by rotating with normal IgG for 1 h at 4 °C. The supernatants were immunoprecipitated with 12.5 μl of each of the beads cross-linked with antibody overnight at 4 °C. The pellets and supernatants were subjected to SDS–PAGE followed by immunoblotting using antibodies against the indicated proteins.

Förster resonance energy transfer (FRET)

Synaptophysin-YFP and pCAGGS-CFP vector were a kind of gift from the Department of Cellular Neurobiology Graduate School of Medicine University of Tokyo. CFP–DJ-1 and CFP–VAMP2 were generated by fusing in frame to the DJ-1 N-terminal or VAMP2 N-terminal coding region in the pCAGGS-CFP vector. HeLa cells were transfected with expression vectors for CFP–DJ-1 or CFP–VAMP2, and synaptophysin-YFP using FuGene HD (Roche), according to the manufacturer's instruction. After 24 h, the cells were imaged with an IX70 inverted microscope (Olympus, Tokyo, Japan) equipped with BioPoint MAC5000 excitation and emission filter wheels (Ludl Electronic Products Ltd., Hawthorne, NY) and a Cool SNAP-HQ cooled CCD camera (Roper Scientific, Trenton, NJ). The filters used were purchased from Omega Optical Inc. (Brattleboro, VT): two excitation filters, XF1071 (440AF21) for CFP and Förster resonance energy transfer (FRET), and XF1068 (500AF25) for YFP; an XF2034 (455DRLP) dichroic mirror; two emission filters, XF3075 (480AF30) for CFP and XF3079 (535AF26) for FRET and YFP. Cells were illuminated with a 75 W xenon lamp through a 6% ND filter. Exposure times for 3×3 binning were 100 ms to obtain fluorescence images and 20 ms to obtain differential interference contrast image. MetaMorph software (Universal Imaging, West Chester, PA) was used to control the CCD camera and filter wheels, and also for the analysis of the cell image data.

Sensitized FRET measurement was performed using the method by Gordon et al.(1998). Briefly, fluorescence images for more than 20 cells were acquired sequentially through YFP, CFP, and FRET filter channels. The background was subtracted from raw images before FRET calculations. The fractions of the bleed-through of CFP and YFP fluorescence through the FRET channel were 0.502 and 0.385, respectively. Corrected FRET ($FRET_C$) was therefore calculated on a pixel-by-pixel basis for the entire image by using the equation: $FRET_C = FRET - 0.502 \times CFP - 0.385 \times YFP$, where FRET, YFP, and CFP correspond to background-subtracted images of cells co-expressing CFP and YFP. Calculated $FRET_C$ values are expressed as box and whisker plots, where the highest and lowest boundaries of the box represent the 25th and 75th percentiles, respectively, and whiskers above and below the box designate the 10th and 90th percentiles, respectively; the line within the box indicates the median value. $FRET_C$ images are also presented in the pseudocolor mode.

Alternatively, 293F cells (Invitrogen) were transfected with expression vectors for CFP–DJ-1 or CFP–VAMP2, and synaptophysin-YFP using 293fectin (Invitrogen) according to the manufacturer's recommendation. After 24 h, the cells were analyzed by a Flicyme-300 flow cytometer (Mitsui engineering and Shipment, Tokyo, Japan), which is equipped with a 445 nm semiconductor laser and is able to measure the fluorescence lifetime of CFP in the frequency domain at a single cell level. Data were acquired using the machine-bundled software, and exported to FlowJo flow cytometry analysis software (Tree Star, Inc., Ashland, OR). Using a gate tool, a population that expresses both CFP and YFP was selected, and FRET efficiency (E) of each cell was calculated by the following equation: $E = 1 - \tau_d'/\tau_d$, where, τ_d' and τ_d are donor (CFP) lifetimes in the presence and absence of the acceptor chromophore, respectively. E values of all analyzed cells were plotted in box and whisker plots.

Confocal laser scanning microscopy

Confocal images were obtained using an FV-10i confocal microscope (Olympus, Tokyo, Japan). Image data were exported to MetaMorph software and fluorescence intensities on lines of interest were gauged by the "Line Scan" function and plotted.

Cell fractionation

For cell fractionation studies, cultured cells (PC12) were washed with PBS, scraped off the culture plate in PBS, and centrifuged at 600*g* for 5 min. Cell pellets were resuspended in homogenization buffer (20 mM HEPES pH 7.2 and 0.25 M sucrose) in the presence of a cocktail of protease inhibitor (Complete Mini, EDTA-free), and sonicated at 4 °C (10 s, 3 times). The nuclei and unbroken cells were then pelleted by centrifugation at 1000*g* for 10 min at 4 °C. The supernatant was centrifuged at 100,000*g* for 1 h at 4 °C to separate the cytosolic and membrane fractions. To study the effects of salts and non-ionic detergent on the solubilization of DJ-1, the membrane fractions were incubated on ice for 30 min with homogenization buffer with 50, 150, and 1000 mM sodium chloride or 1% Triton X-100. After separation of the soluble and insoluble materials by centrifugation (100,000g, for 1 h, at 4 °C), equal volumes of each fraction were subjected to immunoblot with DJ-1, Parkin, and Tfn-R antibodies.

Proteinase K (PK) digestion of PC12 cell membrane fractions

Membrane fractions were isolated from PC12 cells and incubated with 0, 20, 40, 60, 80, and 120 μl of Proteinase K (PK)-agarose (Sigma) at 30 °C with rotation for 1 h. PK beads were removed from the

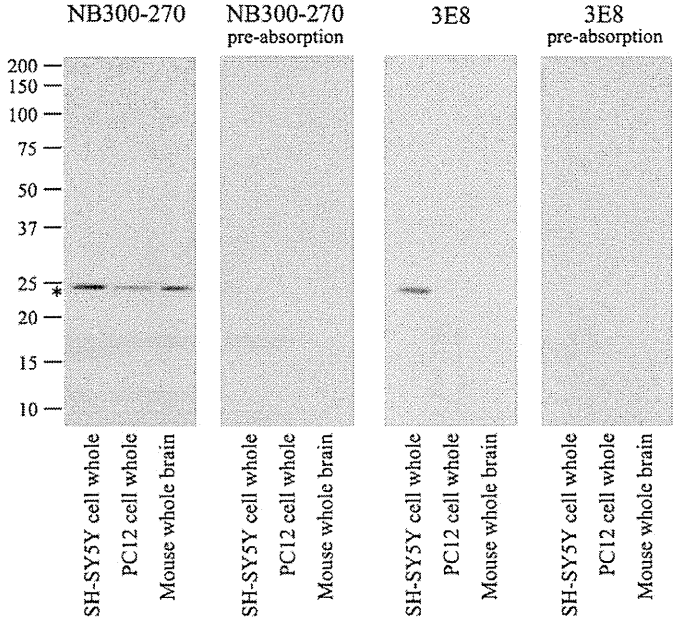

Fig. 1. Characterization of anti-DJ-1 antibodies. (A) Immunoblot of lysates from SH-SY5Y cells, PC12 cells, and mouse whole brain. Commercially available DJ-1 rabbit polyclonal antibody and mouse monoclonal antibody were used, as mentioned in Materials and methods. Specificities of these antibodies were confirmed by pre-absorption tests.

reacted membrane by centrifugation 5 times. PK-treated membranes were subjected to electrophoresis through Tris–HCl polyacrylamide gels (BIO-CRAFT) followed by staining with the GelCode SilverSNAP Stain Kit (Pierce).

In vitro binding assay by PC12 membranes

Recombinant DJ-1 WT, fused at its N terminus to the GST protein, or GST protein for negative control, were reacted with PC12 membranes, or PK-treated membranes (120 μl of PK beads concentration), at 30 °C for 1 h. The reacted samples were centrifuged at 100,000*g* for 1 h at 4 °C, and divided into supernatant and pellet. Both supernatant and pellet were subjected to SDS–PAGE followed by immunoblotting.

In vitro binding assay by LS1 fraction from DJ-1 KO mice

GST–DJ-1 WT recombinant protein (500 nM) or GST–DJ-1 mutant recombinant protein (M26I, A104T, D149A, and L166P) were combined with 200 μl of the LS1 fraction from DJ-1 KO mice ($n=3$), and rotated at 30 °C for 20 min. After treatment, the samples were centrifuged at 260,000*g* for 2 h at 4 °C. The supernatants were extracted and equal volumes of each fraction were subjected to immunoblot with anti-GST antibodies. The pellets were resuspended with the buffer (0.32 M sucrose-HEPES (pH 7.4) buffer) of equal volume, and equal volumes of each fraction were also subjected to immunoblot.

Immunoblotting

Cell lysates were mixed with LDS sample buffer (Invitrogen), heated for 5 min at 95 °C, and incubated on ice. The samples were resolved on 10–20% Tris–HCl gel (BIO CRAFT) in 1% SDS buffer and transferred onto polyvinylidene fluoride membranes (Bio-Rad Bioscience; Hercules, CA). The membranes were blocked for 1 h in TBS containing 0.1% Tween-20 (TBS-T) and 5% non-fat milk (BD Disco), and then incubated overnight at 4 °C with the primary antibody. The membranes were washed with TBS-T 3 times, followed by incubation for 1 h at RT with horseradish peroxidase-conjugated anti-mouse or anti-rabbit IgG. Immunoreactivity (IR) was assessed by a chemiluminescence reaction using Western Lightning (Perkin Elmer-Cetus, Foster City, CA) or ECL Plus reagent (GE Health Care Bio-Sciences).

Results

Characterization of anti-DJ-1 antibodies

To determine the endogenous localization of DJ-1, we employed the use of the commercially available mouse monoclonal and rabbit polyclonal DJ-1 antibodies. Immunoblot analyses using NB300-270 antibody (a rabbit polyclonal antibody) revealed a single band around 22 kDa corresponding to endogenous DJ-1 in the extracts from SH-SY5Y cells, PC12 cells, and mouse brain (Fig. 1). The 3E8 antibody, a mouse monoclonal antibody, also recognized a single band corresponding to the human DJ-1 protein in SH-SY5Y cells. However, this antibody did not detect the rodent DJ-1 protein in PC12 cells and mouse brain (Fig. 1). The band corresponding to DJ-1 disappeared when the antibody was pre-incubated with an excess amount of the antigen, confirming the specificity of the antibody (Fig. 1). Based on these results, the 3E8 antibody, which specifically recognizes endogenous human DJ-1, was used for immunocytochemistry, and the polyclonal NB300-270 antibody, which recognizes the mouse and rodent DJ-1 protein, was used for immunoblotting and immunocytochemistry of primary cortical neuronal cells obtained from mouse brain.

DJ-1 diffusely distributes with main membranous organelles

To examine the subcellular localization of DJ-1, SH-SY5Y cells were double-stained with the DJ-1 antibody and organelle-specific antibodies. Microscopic observation revealed diffuse DJ-1 immunostaining and the protein partly colocalized with GM130, a marker for Golgi apparatus. A small portion of DJ-1 colocalized with Mito Tracker and Tom20, both mitochondrial markers, and calnexin, an ER marker (Fig. 2A).

Based on the immunocytochemical data showing diffuse distribution of DJ-1 in cultured cells, we investigated the precise localization of DJ-1 using biochemical methods. To elucidate DJ-1 distribution in neuronal cells, mouse brain samples were fractionated by differential centrifugation and the fractions were analyzed for the presence of DJ-1 by immunoblotting (Fig. 2B). DJ-1 was present at considerable levels in the synaptosomes (P2′), which consisted of synaptic terminals including synaptic plasma membranes (LP1) and synaptic vesicles (LP2), and co-fractionated with synaptophysin, synaptotagmin, and

Fig. 2. DJ-1 was widely distributed with the main membranous organelles and synaptosomes. (A) SH-SY5Y cells were double-stained with antibodies to DJ-1 (green) and Mito Tracker, Tom20 (mitochondria), GM130 (Golgi apparatus), or calnexin (ER). Scale bars = 10 μm. (B) The experimental design of the synaptosome preparation is shown. (C) Subcellular fractionation of the mouse brain is described in Materials and methods. Aliquots of the subcellular fractions, containing 5 μg of protein, were analyzed by immunoblotting. NR-1 (membrane marker) was recognized in the LP1 fraction, and synaptophysin, synaptotagmin, and VAMP2 (vesicle marker) were detected in the LP2 fraction. Rab3A, Rab4A, Rab5B and Rab7B were widely concentrated in various subcellular fractions. DJ-1 was found in various fractions in conjunction with the Rab proteins. (D) Complex I–V (mitochondria), and GM130 (Golgi apparatus) organelle markers were investigated. Mitochondria were present in the P2′ and the LP1 fractions, but mitochondria were barely evident in the synaptic fraction. The Golgi fraction did appear in the cytosolic fraction (S2). (E) The amount of each fraction was quantified and graphed as a percentage for the estimated amount of whole brain protein. Data were the average ± SD of three independent experiments. (F) Using the results from panel C, immunoreactivity (IR) of each fraction was quantified and graphed as a percentage of each IR to the total immunoreactivities in DJ-1. Synaptophysin and NR-1 were compared with DJ-1 as well.

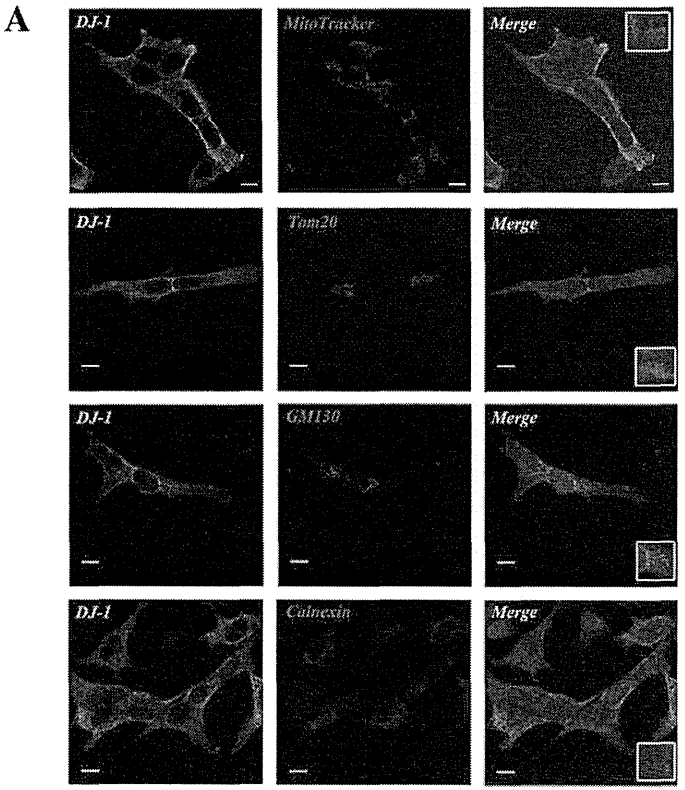

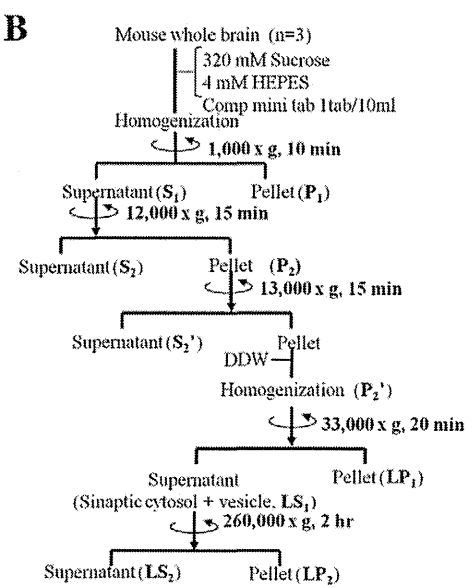

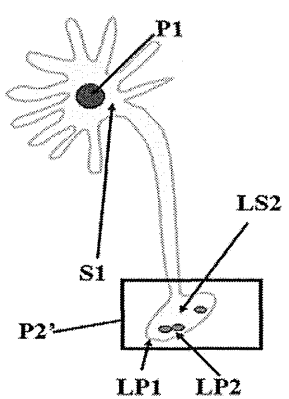

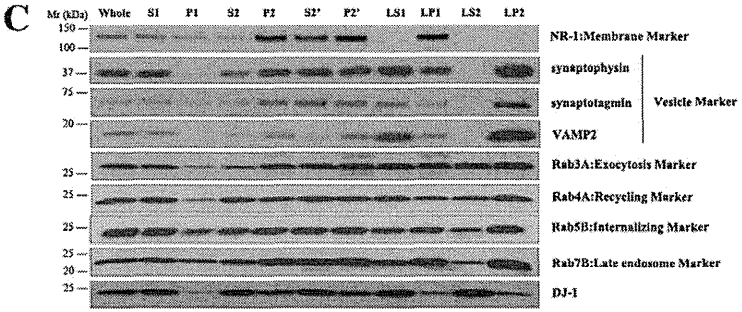

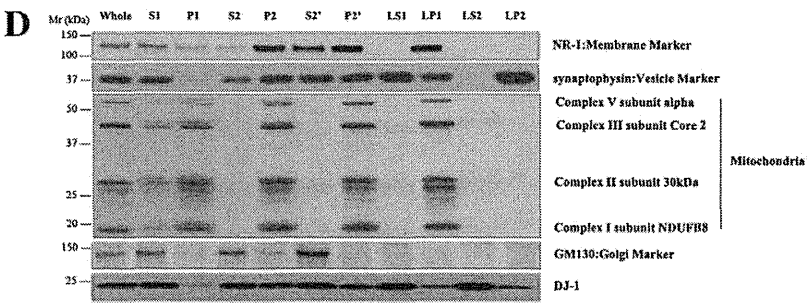

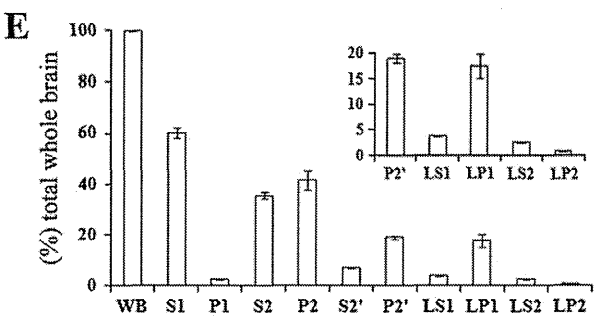

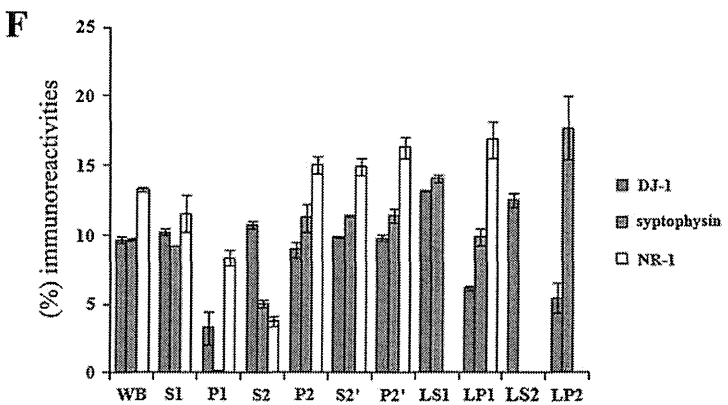

VAMP2 (Fig. 2C). To further characterize the distribution of DJ-1 within synaptosomes, we investigated members of the family of monomeric GTPases called Rab proteins, such as Rab3A (exocytosis marker), Rab4A (recycling marker), Rab5B (endosome marker), and Rab7B (late endosome marker). As shown in Fig. 2B, these Rab proteins co-fractionated with DJ-1. However, mitochondrial respiratory complex proteins (Complex I subunit NDUFB8, Complex II subunit 30 kDa, Complex III subunit Core 2, and ATP synthase (Complex V) subunit α), which are mitochondrial markers, and the Golgi apparatus protein GM130, were not concentrated in the synaptic vesicle fraction (LP2) (Fig. 2D). The amount of each fraction was quantified and expressed as a percentage for the estimated amount of whole brain protein. The percentage of the P1 fraction was $2.69 \pm 0.20\%$, and DJ-1 was present in the nucleus, even though it was small. The percentages of P2′, LS1, LP1, LS2, and LP2, were $19.07 \pm 0.80\%$, $3.71 \pm 0.08\%$, $17.58 \pm 2.36\%$, $2.46 \pm 0.11\%$, and $0.75 \pm 0.19\%$, respectively (Fig. 2E). The amount of protein in the LP2 fraction was much less than that of the whole brain. DJ-1 IR of each fraction was quantified and shown as a percentage of each IR to total immunoreactivities. The percentage of DJ-1 IR of each fraction was $9.82 \pm 0.22\%$ (P2′), $13.19 \pm 0.07\%$ (LS1), $6.18 \pm 0.20\%$ (LP1), $12.54 \pm 0.50\%$ (LS2), and $5.43 \pm 1.08\%$ (LP2) (Fig. 2F).

DJ-1 localized on synaptic vesicles associated with synaptophysin and Rab3A

DJ-1 distributed with synaptic vesicles in the mouse brain (Fig. 2C). To elucidate the vesicle localization of DJ-1, the LS1 fraction containing synaptic vesicles and cytosol from mouse brain was further fractionated by sucrose density gradients centrifugation. Synaptophysin, VAMP2, synaptotagmin, and several Rab proteins were seen in fractions 9–18, and therefore, synaptic vesicles were collected in these fractions (Fig. 3A, B). Otherwise, the immunoreactivities of the synaptic vesicle markers were absent in fractions 1–8, suggesting that they were cytosolic fractions. The distribution of DJ-1 displayed biphasic peaks of both cytosolic fractions (fractions 1–8) and vesicle fractions (fractions 12–14). Coincidentally, the peak of DJ-1 IR agreed with the latter peak of synaptophysin and Rab3A (Fig. 3A, B). To further investigate the colocalization between DJ-1 and synaptic vesicles in neurons, primary cortical neuronal cells obtained from mouse brain were double-stained for DJ-1, and for synaptophysin or Rab3A. DJ-1 immunostaining appeared as punctate structures in the cytosol, axon, and synaptic terminals. DJ-1 was found to partly colocalize with synaptophysin and Rab3A, which play important roles in exocytosis (Edelmann et al., 1995; Handley et al., 2007) (Fig. 3C).

To gain further insight into the vesicle localization of DJ-1, immunoisolation was performed, as previously described (Burre et al., 2007; Morciano et al., 2005), with the LS1 fraction containing synaptic cytosol and vesicles from the mouse brain (Fig. 4A). To remove the nonspecifically interacting material, the LS1 fraction was treated with antibody-linked magnetic beads (Dyna-beads), which are cross-linked with normal rabbit or mouse IgG, and then the beads were removed. It was confirmed that DJ-1 and synaptophysin were not lost under this condition (Fig. 4B). Pre-cleaned LS1 was incubated with the Dyna-beads cross-linked with the DJ-1 antibodies, and then the vesicle isolates containing DJ-1 were subjected to immunoblotting with the DJ-1 antibody. Interestingly, synaptophysin and VAMP2 also localized with the DJ-1-associated vesicles (Fig. 4C). HSP70, which is known as a nuclear and cytosolic protein (Daugaard et al., 2007), was not isolated by this procedure (Fig. 4C). This indicates that the synaptic vesicle fraction was not contaminated with the cytosolic fraction. Therefore, this suggests that DJ-1, synaptophysin, and VAMP2 might localize on the surface of the same vesicle. In addition, it was further investigated whether DJ-1 directly interacts with synaptophysin and/or VAMP2. The LS1 fraction treated with RIPA buffer was immunoprecipitated with pull-down beads cross-linked

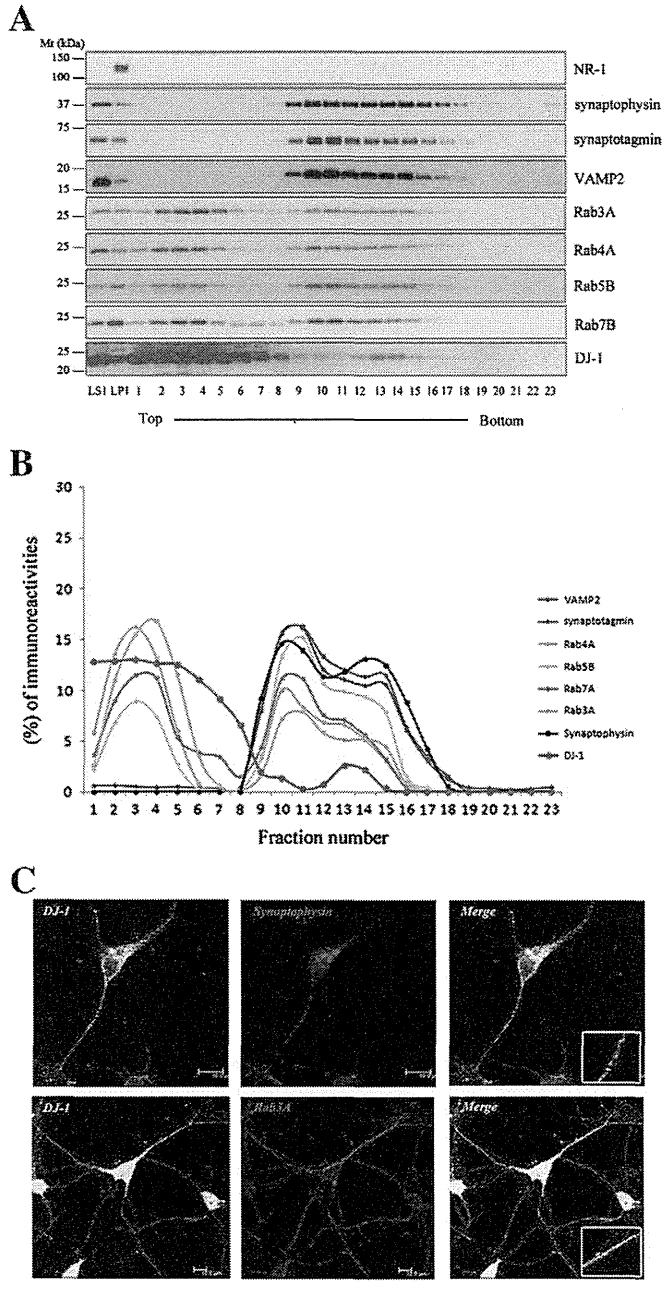

Fig. 3. DJ-1 associates with synaptic vesicles and colocalizes with synaptophysin and Rab3A. (A) The LS1 fraction was layered on top of a linear sucrose density gradient ranging from 0.2–2.0 M sucrose dissolved in HEPES buffer. Fractions were collected and 15 μl of each fraction were subjected to SDS–PAGE followed by immunoblotting using various markers. (B) Using the results from panel A, IR of each fraction was quantified and graphed as a percentage of each IR to the total immunoreactivities in each marker. DJ-1 had a biphasic profile of the immunoreactivities in fractions 1–8 and fractions 12–14, which indicated that there was some cytosolic fraction and some vesicle fractions. The peak of DJ-1 IR was in agreement with the latter peak of synaptophysin and Rab3A. (C) Primary cortical neurons from the mouse brain were fixed, permeabilized, and immunostained with DJ-1 antibody, and double-stained for synaptophysin and Rab3A. DJ-1 overlapped with synaptophysin and Rab3A. Scale bars = 10 μm.

with the synaptophysin antibody. It was found that VAMP2 interacts with synaptophysin as previous studies had reported (Baumert et al., 1989; Edelmann et al., 1995; Trimble et al., 1988). Immunoblotting with DJ-1 antibodies did not reveal endogenous DJ-1 in the resultant immunoprecipitates (Fig. 4C), whereas, endogenous synaptophysin and VAMP2 were not immunoprecipitated with the DJ-1 antibody.

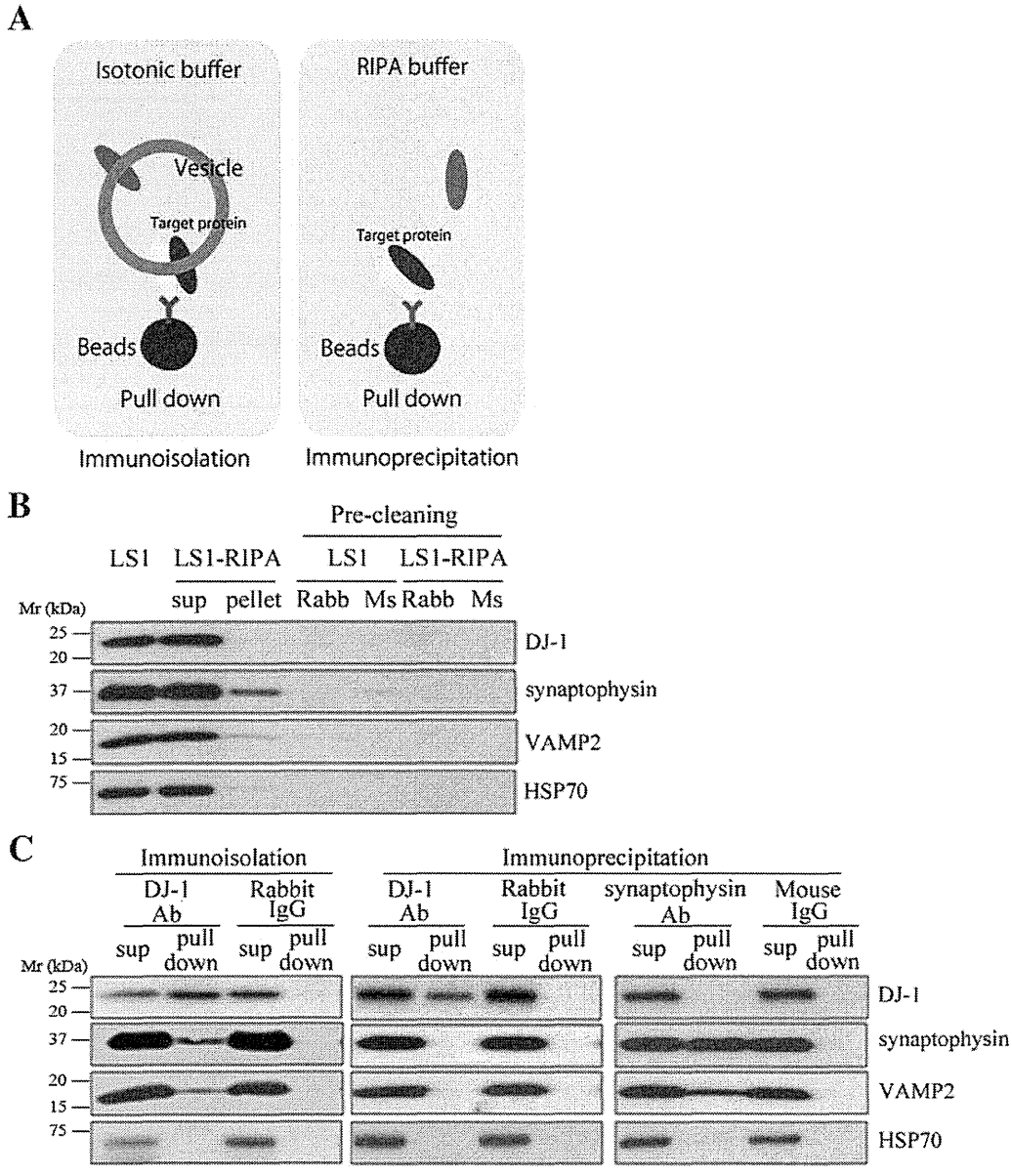

Fig. 4. DJ-1 cannot directly interact with synaptophysin and VAMP2, but associates with the same synaptic vesicles. (A) Image of immunoisolation and immunoprecipitation. Immunoisolation was used to pull down the target protein from the subcellular organelles (synaptic vesicle) from the homogenate, which was reacted with the isotonic buffer. Meanwhile, immunoprecipitation was used to pull down the target protein from the homogenate, which reacted with the buffer containing the detergent in order to examine the direct interactions between proteins. These methods were then used to assess the protein localized on the subcellular organelles with the target protein. (B) The LS1 fraction was first pre-cleaned. To remove nonspecifically-binding material, the LS1 fraction was treated with Dyna-beads cross-linked with normal rabbit or mouse IgG. It was confirmed that the targeting proteins were not lost in this reaction. (C) Sucrose buffer or RIPA buffer extracts of the mouse brain synaptic vesicle fractions were immunoisolated or immunoprecipitated using Dyna-beads coated with each antibody. Immunoisolates, immunoprecipitates and their corresponding supernatants were subjected to SDS–PAGE followed by immunoblotting using antibodies against the indicated proteins. Synaptophysin and VAMP2 were immunoisolated using Dyna-beads coated with the DJ-1 antibody, but they were not immunoprecipitated with the same bead slurry. Sup, supernatant.

Consequently, this proves that DJ-1 cannot directly interact with synaptophysin and VAMP2, but colocalizes with them on the same vesicles.

FRET analyses were performed to examine whether DJ-1 interacts with synaptophysin. We confirmed that FRET occurred between CFP–VAMP2, considered as positive control and synaptophysin-YFP (Pennuto et al., 2002). However, FRET was detected only in a small proportion of HeLa cells expressing CFP–DJ-1 and synaptophysin-YFP (Fig. 5A). $FRET_C$ median values with CFP–VAMP2, CFP–DJ-1, and CFP alone for more than 20 cells, were expressed as 0.363, 0.0413, and 0.0163, respectively (Fig. 5B). 293F cells expressing CFP–VAMP2 or CFP–DJ-1 and synaptophysin-YFP were also subjected to fluorescence lifetime flow cytometry, and fluorescence lifetimes of more than 10,000 cells in each sample were measured. Again, FRET efficiency observed between DJ-1 and synaptophysin was substantially lower than that between VAMP2 and synaptophysin, but significantly higher than that of the control (Fig. 5C). Confocal microscopic analyses revealed that CFP–DJ-1 also merged with synaptophysin-YFP. This pattern is similar to the colocalization between CFP–VAMP2 and synaptophysin-YFP (Fig. 5D, E). These results indicate that DJ-1 is able to localize with synaptophysin-positive vesicles and may interact with synaptophysin in living cells.